forests

Article

Dominance of Topography on Vegetation Dynamics in the Mt. Qomolangma National Nature Reserve: A UMAP and PLS-SEM Analysis

Binni Xu [1], Jingji Li [1,2,*], Xiangjun Pei [1,2], Lijiao Bian [2], Tingbin Zhang [3], Guihua Yi [4], Xiaojuan Bie [4] and Peihao Peng [4]

[1] State Key Laboratory of Geohazard Prevention and Geoenvironment Protection, Chengdu University of Technology, Chengdu 610059, China; xubinni99@stu.cdut.edu.cn (B.X.); peixj0119@tom.com (X.P.)
[2] College of Ecology and Environment, Chengdu University of Technology, Chengdu 610059, China; bianlijiao@163.com
[3] College of Earth Science, Chengdu University of Technology, Chengdu 610059, China; zhangtb@cdut.edu.cn
[4] College of Tourism and Urban-Rural Planning, Chengdu University of Technology, Chengdu 610059, China; yigh@cdut.edu.cn (G.Y.); biexiaojuan06@cdut.cn (X.B.); peihaop@163.com (P.P.)
* Correspondence: lijingji2014@cdut.edu.cn

Abstract: The southern portion of the Qinghai–Tibet Plateau (QTP) and the central Himalayan region are home to the Mt. Qomolangma (Everest) National Nature Reserve (QNNR), which is the world's highest nature reserve and is distinguished by delicate natural ecosystems and unique geographic features. Analyzing regional vegetation trends, as well as the impacts of natural and anthropogenic variables on vegetation coverage, is crucial for local environmental protection and sustainable development. In this study, the variation patterns of the MOD13Q1 Normalized Difference Vegetation Index (NDVI) data were explored, and the responses of vegetation development to both natural and anthropogenic parameters were investigated by applying trend analysis and partial correlation analysis, as well as the partial least squares-structural equation model (PLS-SEM). To better comprehend the spatial characteristics and interrelationships between NDVI and various parameters under different vegetation types, the Uniform Manifold Approximation and Projection (UMAP) was employed for dimensionality reduction and visualization. The results illustrated that between 2000 and 2018, the reserve greened up at a rate of 0.00073/a ($p < 0.05$), with vegetation improvement areas accounting for 49.46%. The major climatic driver for the greening trend of vegetation was temperature. Topography (especially elevation) remains dominant in regulating vegetation development in the QNNR, despite a progressively growing impact of hydrothermal conditions on vegetation development. Additionally, the implementation of environmental initiatives has stifled the adverse impacts of human activity.

Keywords: vegetation dynamics; climate change; anthropogenic activity; terrain; uniform manifold approximation and projection (UMAP); partial least squares structural equation model (PLS-SEM)

Citation: Xu, B.; Li, J.; Pei, X.; Bian, L.; Zhang, T.; Yi, G.; Bie, X.; Peng, P. Dominance of Topography on Vegetation Dynamics in the Mt. Qomolangma National Nature Reserve: A UMAP and PLS-SEM Analysis. *Forests* **2023**, *14*, 1415. https://doi.org/10.3390/f14071415

Academic Editor: Ramón Alberto Díaz-Varela

Received: 9 June 2023
Revised: 29 June 2023
Accepted: 8 July 2023
Published: 11 July 2023

1. Introduction

The balance of the terrestrial ecosystem is maintained by vegetation [1], which is a vital connection of the atmosphere, hydrosphere, and soil [2] that results from the long-term interactions between climate, terrain, and human activity [3–5]. The structure and dynamics of terrestrial natural systems have been strongly influenced by global warming in the last few decades, particularly in alpine and subalpine forest communities where vegetation variations are more responsive to topography [6–13]. According to research, the combined effects of terrain and climate are what lead to the regional variability of vegetation [14,15]. The spatial distribution of water, temperature, and radiation, as well as nutrients, is influenced by topography in mountainous regions with extreme elevation differences [16,17].

Thus, both directly and indirectly, the terrain has an impact on vegetation dynamics. In the northeastern Tibetan Plateau, the dominant factors driving vegetation changes were determined to be annual average temperature, soil type, and elevation, which explained over 15% of the variation [18]. The coevolution of vegetation should be comprehensively investigated with topography, climate, and soil conditions to further restore degraded ecosystems and maintain ecosystem diversity [19]. Previous studies have demonstrated that temperature and precipitation are the main elements influencing the dynamics of vegetation, and appropriate warming has a favorable impact on vegetation cover [20,21]. Specifically, in the southeast Qinghai–Tibet Plateau, most climatic factors exhibit a unimodal relationship with forest moss plant diversity; when temperature exceeds the optimal threshold for moss plant growth, even minor warming can lead to a decline in moss plant diversity. Temperature factors, especially minimum temperature and daily temperature range, are identified as the most influential drivers of forest moss plant diversity and distribution [22]. While wetness increases soil moisture and air humidity, which could promote the growth of plants [23,24], it also lowers the radiation and temperature that prevent plants from growing [12,25,26]. The mountain ecosystem, with its significant elevation changes, challenges the notion that climatic variables primarily influence vegetation dynamics. Additionally, it is crucial to consider how intensified human activity impacts vegetation coverage [27–29], including the benefits of properly implemented ecological restoration programs that result in improving vegetation cover [30–32]; reducing ecosystem vulnerability and minimizing extreme weather effects [30,33,34]; and the detrimental effects of overgrazing, deforestation, and massive construction projects [34–37]. Thus, investigating the changing patterns of vegetation as well as quantitatively assessing the influence of natural and anthropogenic variables on vegetation variation are crucial for the sustainable development of the reserve [38–40].

The Qinghai–Tibet Plateau (QTP), sometimes referred to as the “Asia Water Tower” and “Earth’s Third Pole” [41,42], is a vast area covered by glaciers and is a powerful source of atmospheric heat [43] that profoundly affects local and global climate change [44,45]. Mt. Qomolangma, located at the southernmost border of QTP, is one of the most dynamic and delicate mountain ecosystems worldwide, which has enormous elevation changes and is extremely vulnerable to both topographic and climatic change [46,47]. Consequently, the Mt. Qomolangma (Everest) National Nature Reserve (QNNR) was formed in 1998 to safeguard the natural resources of the exceptionally high mountain ecosystem, mountain forest ecosystems, shrub and grassland ecosystem, as well as their biological distribution and ethnic, historical, and cultural heritage [48] (Figure 1). The reserve is split into two sections, the southern slope, which contains a semi-humid montane forest system, and the northern slope, where the plateau semi-arid shrub fallow and grassland system are present. Several studies concluded that the increasing rates of temperature and human activity development in the QTP and the QNNR are more rapid compared with the global average level [49–52]. Therefore, the QTP’s and the QNNR’s terrestrial ecology will be permanently impacted as snowpacks steadily diminish [53] and glaciers noticeably thin and recede [41,53–56]. Currently, many studies concentrate on how climate change affects the reserve’s vegetation development [57,58], while few take into account the combined impact of climate, terrain, and anthropogenic activities.

Previously, the multiple linear regression method has been widely utilized to explore the relationship between vegetation response variables (such as phenology, productivity, and NDVI) and various influencing factors. However, this approach may lack the capacity to elucidate the intricate interactions and pathways within the internal system. Moreover, when numerous influencing factors are considered, issues such as overfitting and diminished explanatory value may arise [59,60]. Additionally, the traditional dimensionality reduction method, Principal Component Analysis (PCA), is unable to capture non-linear dependencies between data and may be significantly influenced by potential outliers in the data [61]. To gain a deeper understanding of the clustering behaviors of different types of vegetation under the influence of various factors and to enhance visualization, it is imperative to consider employing the latest non-linear dimensionality reduction techniques. In response to the aforementioned gaps, this study aims to investigate the mechanisms influencing vegetation dynamics by holistically considering the roles of climatic variations, anthropogenic impacts, and the topography of the QNNR. To accomplish this, the partial least squares-structural equation model (PLS-SEM) and Uniform Manifold Approximation and Projection (UMAP) methods were employed. Vegetation variations throughout the growing season of the QNNR were identified using the MOD13Q1 NDVI data, with a 250 m spatial resolution, 16-day temporal interval, and spanning from February 2000 to December 2018. Meteorological data, drawn from the China Meteorological Forcing Dataset (1979–2018) (CMFD), were used to discern the spatiotemporal pattern of climate change throughout the research period.

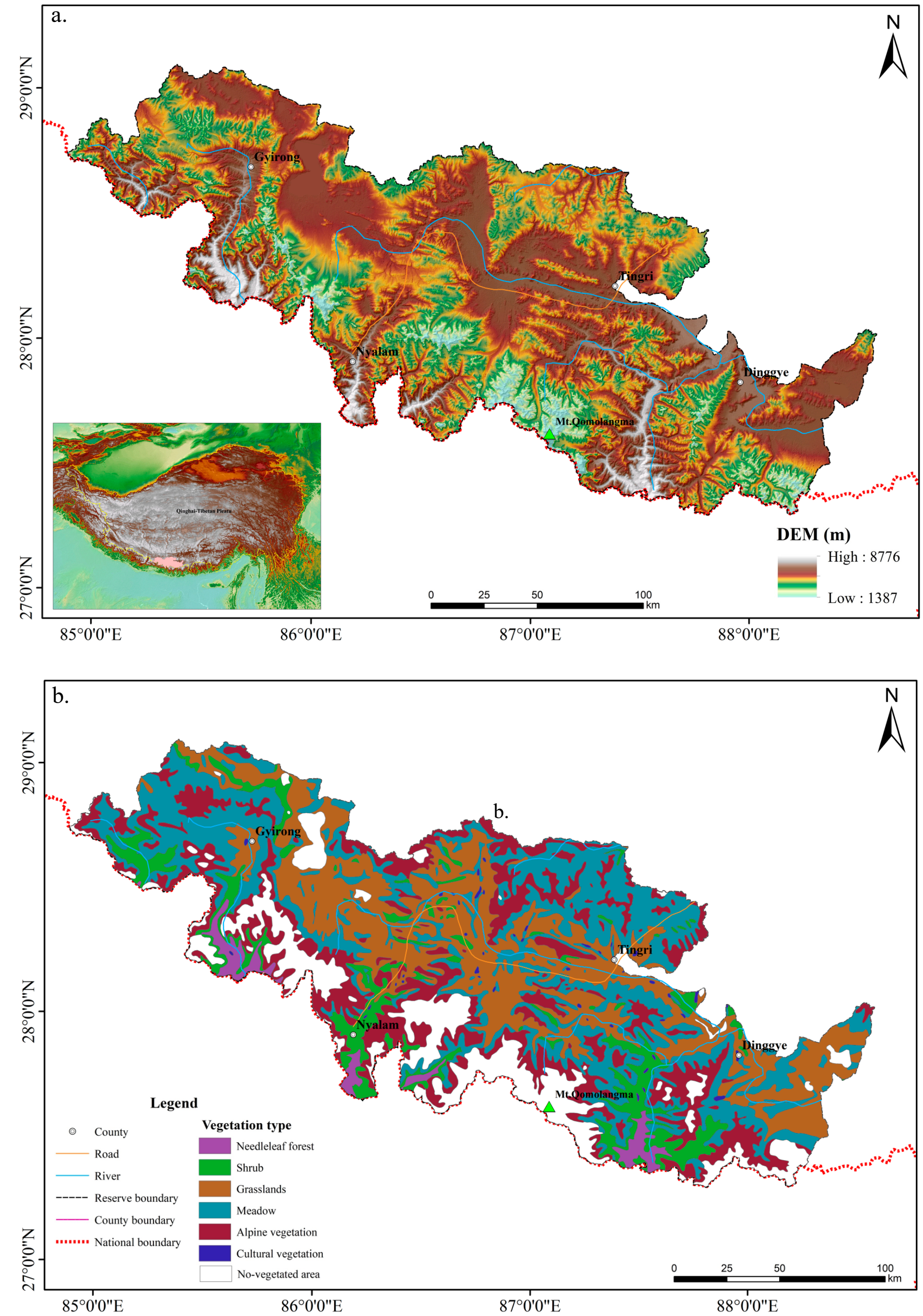

Figure 1. Study area (**a**) and vegetation types (**b**).

By utilizing PLS-SEM and UMAP, a more comprehensive understanding of the intricate interactions between vegetation, natural, and anthropogenic drivers could be achieved. The principal objectives of this study were as follows: (1) to examine the changes in vegetation of the reserve over the past 19 years; (2) to explore the partial correlations between vegetation development and meteorological parameters; and (3) to evaluate the influence of both natural and anthropogenic factors on vegetation variation. By illuminating the underlying mechanisms driving vegetation developments, this study hopes to offer technical support for the sustainable development of the reserve.

2. Materials and Methods

2.1. Study Area

The QNNR, which encompasses the counties of Tingri, Gyirong, Nyalam, and Dinggye, is situated on the boundary of China and Nepal. It has a maximum elevation of 8848.96 m.a.s.l. (Mt. Qomolangma), a minimum elevation of 1440 m.a.s.l., and a total area of 33,819 km^2 (Figure 1a). Centered on Mt. Qomolangma, the reserve is split into the southern slope and the northern slope of the Himalayas, each having considerably distinct weather conditions. During 2000–2018, the mean annual temperatures at Nyalam station (on the southern slope) and Tingri station (on the northern slope) were 4.28 °C and 3.78 °C, respectively, while their respective mean annual precipitation amounts were 613.9 mm and 297.4 mm [62]. Since the Himalayas prevent warm, humid air from the Indian Ocean and the Bengal Bay from reaching the QTP [63], the southern slope of the reserve experiences abundant rainfall and vegetation during the monsoon season, contrasting with the rather arid climate condition on the northern slope. Thus, the southern slope illustrates the semi-humid mountain forest system that is dominated by alpine vegetation (AV) and needleleaf forest (NF). In contrast, the northern slope is primarily covered by shrubs, grassland, and meadow, and features a plateau semi-arid bush fallow and steppe system (Figure 1b) [51].

2.2. Data Source and Pre-Processing

The Normalized Difference Vegetation Index (NDVI) is an efficient indicator that is frequently used in investigations of vegetation activities [12,25]. This study covered the period from February 2000 to December 2018 and used MOD13Q1 NDVI data, which are provided every 16 days at 250-m spatial resolution by the National Aeronautics and Space Administration (NASA, https://ladsweb.modaps.eosdis.nasa.gov/ accessed on 5 February 2023). With the help of the MODIS Reprojection Tool (MTR), the original NDVI data were transformed and projected. The monthly, growing season (April to October), interannual, and average scale NDVI values were all produced using the Maximum Value Composite (MVC) approach. The pixels with NDVI values less than 0.1 were masked out, indicating sparse and non-vegetated places such bare soil, water body, snow, and ice [64].

In this study, thw China Meteorological Forcing Dataset (1979–2018) (CMFD) was used, provided by the National Tibetan Plateau Data Center (https://doi.org/10.11888/AtmosphericPhysics.tpe.249369.file accessed on 7 February 2023) [65] with a spatial resolution of 0.1°, which was generated by combining ground-based observations with a number of gridded datasets from remote sensing and reanalysis using AUSPLIN Statistical interpolation [66]. The four climatic raster datasets including temperature, radiation, precipitation, and specific humidity were selected for further analysis. The total precipitation and radiation of the growth season were obtained by adding up the monthly values from April to October, while the growing season's mean temperature and specific humidity were derived by averaging the monthly values from April to October.

The digitized vegetation map provided by the Resource and Environment Science and Data Center (https://www.resdc.cn/ accessed on 8 February 2023) was used to extract the 1 km resolution vegetation type data. The DEM (30 m resolution) data was collected from the Geospatial Data Cloud (https://www.gscloud.cn/ accessed on 8 February 2023), and elevation, slope and aspect data were extracted from DEM data. The 1 km grid datasets of human activity intensity in agricultural and pastoral areas of the Qinghai–Tibet

Plateau during 1990–2015 were collected from the National Tibetan Plateau Data Center (https://doi.org/10.11888/HumanNat.tpdc.300295 accessed on 7 February 2023) [67].

In this study, the bilinear interpolation method was used to resample all the remote sensing data into 250 m to match the spatial resolution of NDVI. Table 1 illustrates the details of datasets employed in this study.

Table 1. Dataset source.

Dataset	Spatial Resolution	Time Scale	Source
MOD13Q1 NDVI dataset	250 m	2000.02–2018.12	https://ladsweb.modaps.eosdis.nasa.gov/
Climate dataset	0.15° (resampled as 250 m)	1979–2018	https://doi.org/10.11888/AtmosphericPhysics.tpe.249369.file
Vegetation type	1 km (resampled as 250 m)	/	https://www.resdc.cn/
DEM	30 m (resampled as 250 m)	/	https://www.gscloud.cn/
Human activity intensity dataset	1 km (resampled as 250 m)	1990–2015	https://doi.org/10.11888/HumanNat.tpdc.300295

2.3. Methods

Figure 2 shows the flow chart of this study.

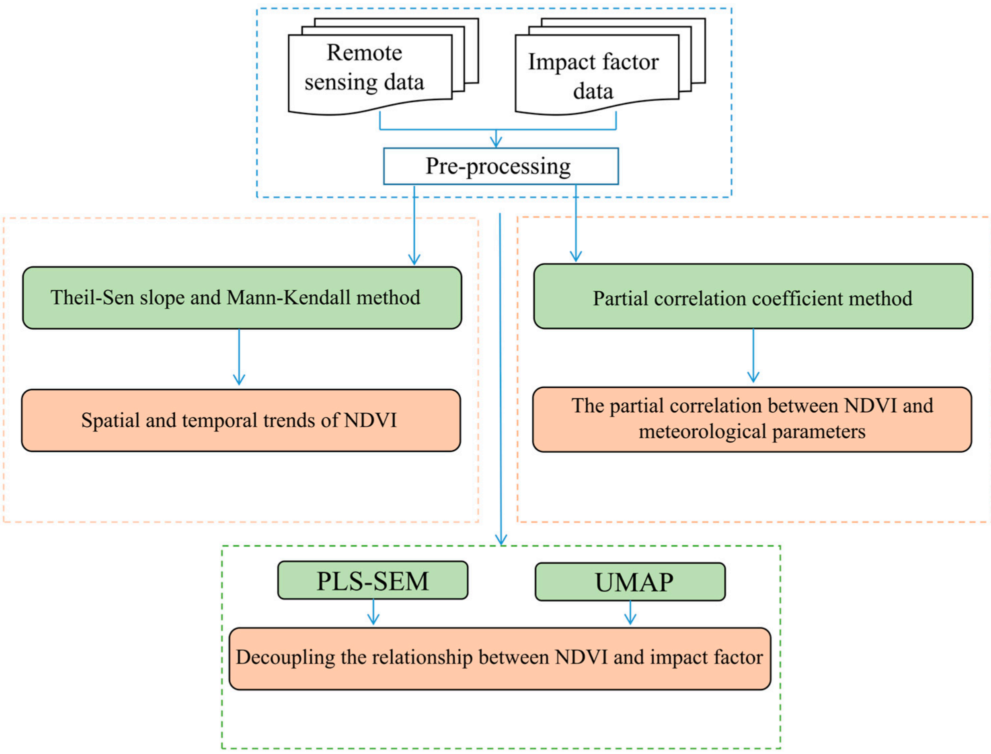

Figure 2. The technical procedures used in the study.

2.3.1. Theil–Sen Median and Mann–Kendall Method

The Theil–Sen median approach is a qualitative approach for assessing the time-series trends that has the advantage of not being affected by the sample absence [68], which was employed in our study to identify variations in vegetation. The following is the calculation equation:

$$\beta = Median\left(\frac{x_j - x_i}{j - i}\right) \quad 0 < i < j < n \tag{1}$$

where, x_i and x_j stand for the NDVI value at the time i and j. n means the data length. $\beta > 0$ depicts an upward trend, while $\beta < 0$ illustrates a downward trend.

The Mann–Kendall approach is a nonparametric statistical technique that has the benefit of allowing the sample to deviate from expected distributions, while taking into account any existing outliers [69]. This approach is widely used for significance tests of vegetation and meteorological trends [70]. The formulas are as follows:

$$S = \sum_{i=1}^{n-1} \sum_{j=i+1}^{n} \mathrm{sgn}(x_j - x_i) \tag{2}$$

$$\mathrm{sgn}(x_j - x_i) = \begin{cases} 1, & x_j - x_i > 0 \\ 0, & x_j - x_i = 0 \\ -1, & x_j - x_i < 0 \end{cases} \tag{3}$$

$$\mathrm{Var}(s) = \frac{n(n-1)(2n+5)}{18} \quad (n \geq 8) \tag{4}$$

$$Z = \begin{cases} \frac{S-1}{\sqrt{\mathrm{Var}(s)}} & S > 0 \\ 0 & S = 0 \\ \frac{S+1}{\sqrt{\mathrm{Var}(s)}} & S < 0 \end{cases} \tag{5}$$

where, corresponding, x_i and x_j stand for the NDVI value at the time i and j. n means the data length. S is the test statistic that obeys the positive-terrestrial distribution. $\mathrm{sgn}(x_j - x_i)$ is the logical discriminant function. $\mathrm{Var}(s)$ means the variance of S. In this study, the confidence level of α = 0.05 was selected for further analysis. Depending on the Mann–Kendall results, the variation was either insignificant ($|Z| < 1.96$) or significant ($|Z| > 1.96$). Therefore, the trends of NDVI were reclassed as five levels (Table 2).

Table 2. The level of NDVI trends.

NDVI Trend Level	β	Z
Significant degradation	≤−0.0005	>1.96
Slight degradation	≤−0.0005	−1.96–1.96
Stable	−0.0005–0.0005	−1.96–1.96
Slight improvement	≥0.0005	−1.96–1.96
Significant improvement	≥0.0005	>1.96

2.3.2. Partial Correlation Coefficient Analysis

The relationships between NDVI and meteorological factors were investigated using partial correlation coefficient (PCC) analysis and the *t*-test approach [71]. The following are the equations:

$$r_{i \cdot j \cdot l_1 \cdot l_2 \ldots l_g} = \frac{r_{i \cdot j \cdot l_1 \cdot l_2 \ldots l_{g-1}} - r_{i \cdot l_1 \cdot l_2 \ldots l_{g-1}} * r_{j \cdot l_1 \cdot l_2 \ldots l_{g-1}}}{\sqrt{\left(1 - r^2_{i \cdot l_1 \cdot l_2 \ldots l_{g-1}}\right) * \left(1 - r^2_{j \cdot l_1 \cdot l_2 \ldots l_{g-1}}\right)}} \; g \leq k-2 \tag{6}$$

$$t = \frac{\sqrt{n-k-1} * r}{\sqrt{1-r^2}} \tag{7}$$

where, r represents the PCC value between a certain meteorological parameter and the NDVI, n means the number of time–series data. k represents the controllable variables, and $n - k - 1$ is the degree of freedom. The PCC significance levels were assessed using the *t*-test at the level of 0.05.

2.3.3. Partial Least Squares Structural Equation Modeling

To measure how climatic conditions, topography, and anthropogenic activities affect vegetation dynamics, the partial least squares-structural equation model (PLS-SEM) was developed. PLS-SEM investigates the connections and path coefficients between variables [72] based on an assumed structure or a recognized mechanism [73]. In order to more effectively address the issues of factors' multicollinearity, PLE-SEM utilizes an iterative solution technique based on the principle of dimensionality reduction in principal component analysis [74]. PLS-SEM aims to maximize the explained variance of the latent endogenous variables by evaluating partial model interactions in an iterative series of normal least squares regressions. This method is preferable to covariance-based structural equation model (CB-SEM) for exploratory research and theory development [75]. The measurement model and the structural model are the two sub-models that make up a PLS-SEM. In the PLS path modeling paradigm, the following equation could be used to represent the linear relationship between each latent variable and its related manifest variables [76]:

$$x_{pq} = \lambda_{pq}\, \xi_q + \epsilon_{pq} \tag{8}$$

where, error term ϵ_{pq} denotes measurement process imprecision and λ_{pq} represents the loading associated for p-th manifest variable in the q-th block.

The structural model analyzes the links between the latent variables, which are expressed as [76]:

$$\xi_j = \sum_{i \neq j} \beta_{ij}\xi_i + \zeta_j \tag{9}$$

where, ζ_j is the inaccuracy in the inner relation and β_{ij} is the path coefficient connecting the i-th exogenous variable to the j-th endogenous variable.

The conceptual model was created using the following assumptions: (1) topographic factors directly affect NDVI, (2) climatic factors directly affect NDVI, (3) human activities directly affect NDVI, (4) topographic factors indirectly affect NDVI by influencing climatic factors, (5) topographic factors indirectly affect NDVI by influencing human activities, (6) meteorological factors indirectly affect NDVI by influencing human activities.

In this study, the models are tested using SmartPLS 3.0, and the significance of path coefficients was determined using a sample size of 5000 [77]. The PLS-SEM evaluation requires the fulfillment of three essential requirements. The first measures the overall model's fit and is presented by the coefficient of determination (R^2) value [78]. The Stone–Geissers coefficient (Q^2) value, which measures the model's predictive usefulness with respect to endogenous latent variables, is the second one [79]. The third one measures the overall model's quality using the goodness of fit (GOF) value [80]. The following table displays the empirical standards (Table 3):

Table 3. Elevation of PLS-SEM fitting.

Criterion	Value	Description
R2	>0.67	Substantial explanatory power
	>0.33	Moderate explanatory power
	>0.19	Weak explanatory power
Q2	>0	A larger value denoting higher prediction accuracy of the model
GOF	0.1	Overall fit of the model is weak
	0.25	Overall fit of the model is medium
	0.36	Overall fit of the model is strong

2.3.4. Uniform Manifold Approximation and Projection (UMAP)

Situations involving high-dimensional data, such as texts, images, biological, and other forms of data, may frequently occur in data analysis and might provide a variety of difficulties [81]. Therefore, the curse of dimensionality refers to a situation where typical statistical models perform poorly when dealing with high-dimensional data because their basic assumptions are violated [82].

Dimensionality reduction is essential for dealing with numerous variables, which not only enables the pretreatment of high-dimensional data but also offers a useful visualization of the data points, providing additional insight into the data structure and potentially significant patterns that may already be apparent at this level of investigation [83]. Linear dimensionality reduction techniques, such as Principal Component Analysis (PCA) or Linear Discriminant Analysis (LDA), are applicable when the distribution of the data or the relationships among the data can be effectively expressed through linear transformations. These techniques operate based on linear algebra, and they assume that the data can be simplified through linear combinations or projections into a linear subspace, which may lead to computationally efficient and easily interpreted results. However, when the data encompass intricate nonlinear relationships, linear dimensionality reduction may fail to effectively preserve these associations [84]. In this study, one dependent parameter (NDVI) and nine independent parameters (elevation, slope, aspect, temperature, radiation, precipitation, specific humidity, grazing intensity, human activity intensity) were involved. Dimensionality reduction methods aim to transform these high-dimensional data into lower-dimensional data, while still retaining the critical data information [85].

Trade-offs are inevitable in the process of dimensionality reduction. To capture and retain the group structure's finer-scale features, it is crucial to employ an appropriate technique. While some methods tend to focus on the maximum variance within the dataset, they might neglect the variance occurring in other directions. Various nonlinear neighbor graph-based dimensionality reduction techniques, such as t-SNE [85,86], have been proposed to circumvent this limitation.

In this study, the Uniform Manifold Approximation and Projection (UMAP) approach was utilized, which introduced in 2018 as a nonlinear dimensionality reduction technique whose primary objective is to capture complex nonlinear structures within high-dimensional data and preserve these structures as much as possible in the reduced-dimensional space [87]. The UMAP is a robust tool for dimensional reduction, providing an excellent means to analyze complex cluster structures. The ranking patterns of each dataset were visualized using the UMAP method.

Before performing the dimensionality reduction analysis, all data underwent a Hellinger transformation [88], since UMAP is based on Euclidean distance measurements. The UMAP technique structures the data in a low-dimensional space using a graphical layout [87]. After generating a high-dimensional graph, the algorithm fine-tunes its low-dimension representation to make it as structurally similar as possible. The minimum distance and number of neighbors are critical UMAP parameters that maintain the global and local structure. In this paper, the number of neighbors was set as 10, with the minimum distance set at the default value.

3. Results

3.1. The Changing Patterns of Vegetation Dynamics in the QNNR

The NDVI across the entire QNNR decreased with fluctuation before 2010 and increased significantly afterward, showing an overall greening trend of 0.00073/a (p = 0.037) during 2000–2018 (Figure 3b). The growing season average NDVI illustrated marked spatial heterogeneity in the QNNR during 2000–2018 (Figure 3a). The high NDVI (>0.8) areas were concentrated in relatively low-elevation parts such as the southern portion of the reserve and regions along rivers, which where dominated by NF and shrub. While the low NDVI (<0.2) areas were distributed throughout the reserve, in areas partly covered by lakes, snow, and glaciers, and dominated by grassland, meadow, and AV. Such a vegetation distribution pattern is comprehensively influenced by topography, climatic divergence, and vegetation type. Additionally, the mean growing season NDVI in the QNNR also indicated markedly vertical zonality, which decreased gradually with the increase of elevation.

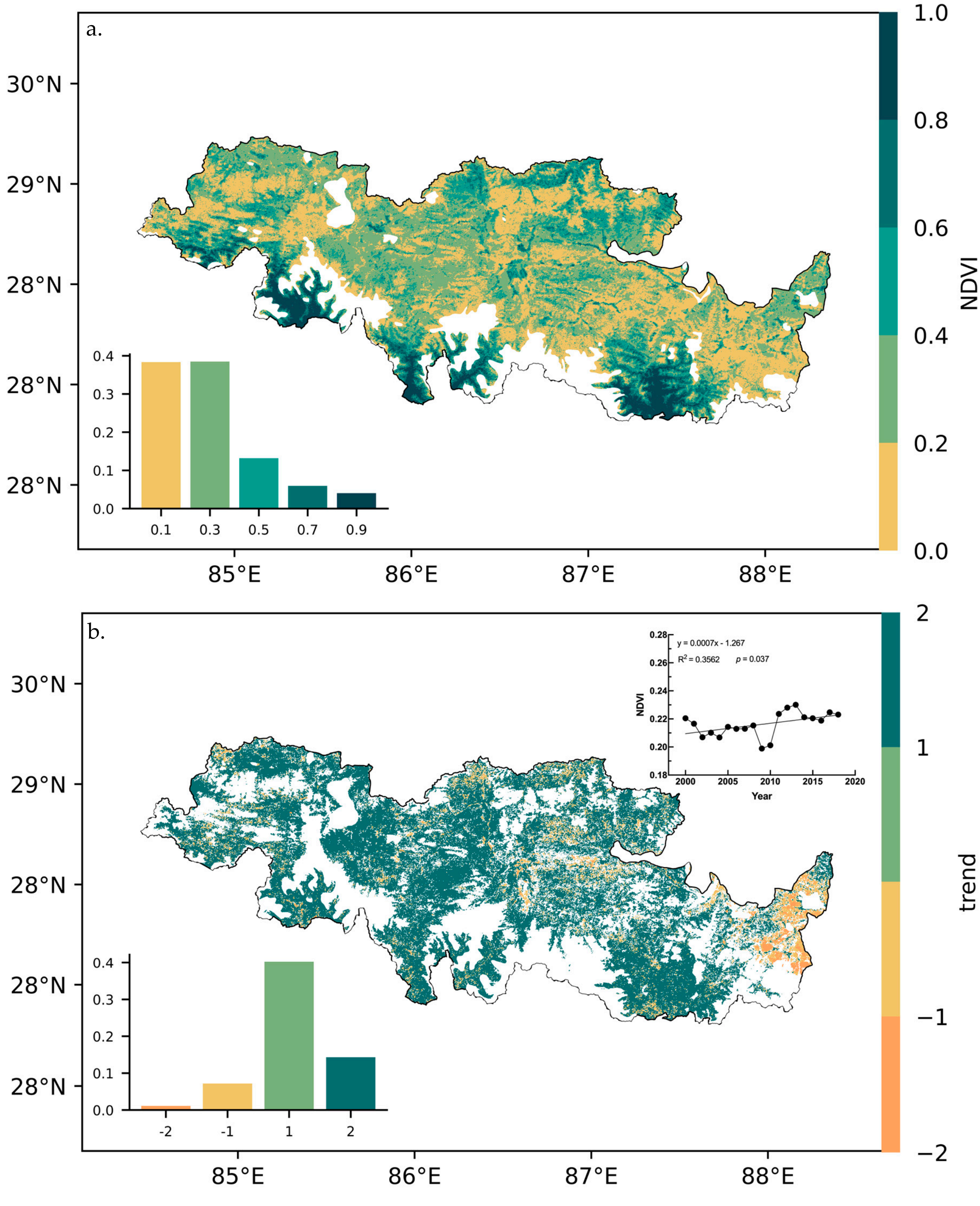

Figure 3. (**a**) The growing season average NDVI pattern, (**b**) the spatial pattern of NDVI trend during 2000–2018 in the QNNR (−2 and −1 indicate significant degradation and slight degradation, while 2 and 1 represent significant improvement and slight improvement, respectively.).

The NDVI changing trend was explored by the Theil–Sen and Mann–Kendall methods (Table 2). Figure 3b showed the NDVI trend characteristics of the study area. In the center of and low-elevation regions on the southern slope of the QNNR, the majority of the areas (40.23%) were slightly improved, where NF, grassland, shrub, and AV dominated. The vegetation stable regions accounted for 37.16% of the areas, and were widely distributed throughout the reserve and mainly dominated by AV vegetation. The areas showing significant improvement (14.31%) were mostly located in the low-elevation area of the southern slope and around lakes and rivers, where abundant hydrothermal conditions and vegetation cover were found. Slight degradation was accounted for in 7.18% of the regions, which were mostly dispersed in the reserve's eastern section and sparsely distributed throughout the study area, where AV dominated. The lowest proportion (1.12%) showed significant degradation. These areas were concentrated in the eastern part of the QNNR, were surrounded by slight degradation areas, and were mainly covered by grassland and possibly affected by human activities such as grazing (Figure 3b). In terms of different elevation levels, the proportions of areas indicated vegetation improvement decreased with increasing elevation, but significant degradation regions were largely concentrated in the middle and low-altitude regions (4000–4500 m), which were dense with human activity.

3.2. The Respond of Vegetation Dynamics to Climate Change in the QNNR

To explore the vegetation dynamic response to a particular climatic variable, the PCC and significance between hydrothermal variables and NDVI during the growing season were investigated at a pixel size.

During 2000–2018, growing season NDVI and hydrothermal parameters' partial correlation levels showed markedly spatial heterogenicity (Figure 4). Specifically, as seen in Figure 4e, the vegetation coverage of the eastern part of the QNNR was negatively correlated with temperature, but the western region's vegetation cover was mostly associated positively with temperature. The positive relation level increased with the rise of elevation, and no obvious difference between the various vegetation types was noted. The level of partial connection between NDVI and radiation is shown in Figure 4g; around glacial lakes in the northwest of the QNNR, the negatively correlated pixels were scattered, while the significant positive association pixels, which made up 2.11% of the total, were dispersed sporadically among the low-elevation areas of the south slope. There was no marked variation in terms of elevation gradient, and grassland was more negatively affected by radiation than other vegetation types. Figure 4a illustrates that NDVI and precipitation are positively correlated in more than 60% of the pixels, with the geographic distribution of high values in the middle and low values in the periphery running from northeast to southwest. The northwest and northeastern corners of the reserve held the majority of the strongly positively associated pixels, and the low elevation zones of the south slope were where the majority of the pixels having a strong negative correlation were located. The percentage of positive correlation grew as elevation climbed. When compared to other types of vegetation, the AV had a more substantial positive correlation with precipitation, which was strongly tied to the distribution characteristics' altitudinal gradient. The distribution pattern of the relationship between vegetation dynamics and specific humidity (Figure 4c) seemed to be comparable to that of radiation (Figure 4g), with a more significant negative correlation with a trend of initial increase followed by a subsequent decrease with increasing elevation. Grassland showed a more pronouncedly negative relationship with specific humidity.

3.3. Quantification of Climate Change, Topography, and Anthropogenic Activities' Impacts on Vegetation Dynamics

3.3.1. Partial Least Squares Structural Equation Model (PLS-SEM)

To more precisely measure how natural and artificial variables interact to affect vegetation growth, a PLS-SEM was established including four climatic parameters (temperature, radiation, precipitation, and specific humidity), three topographic factors (elevation, slope, aspect), and two human activities indicators (human activity intensity, and grazing intensity).

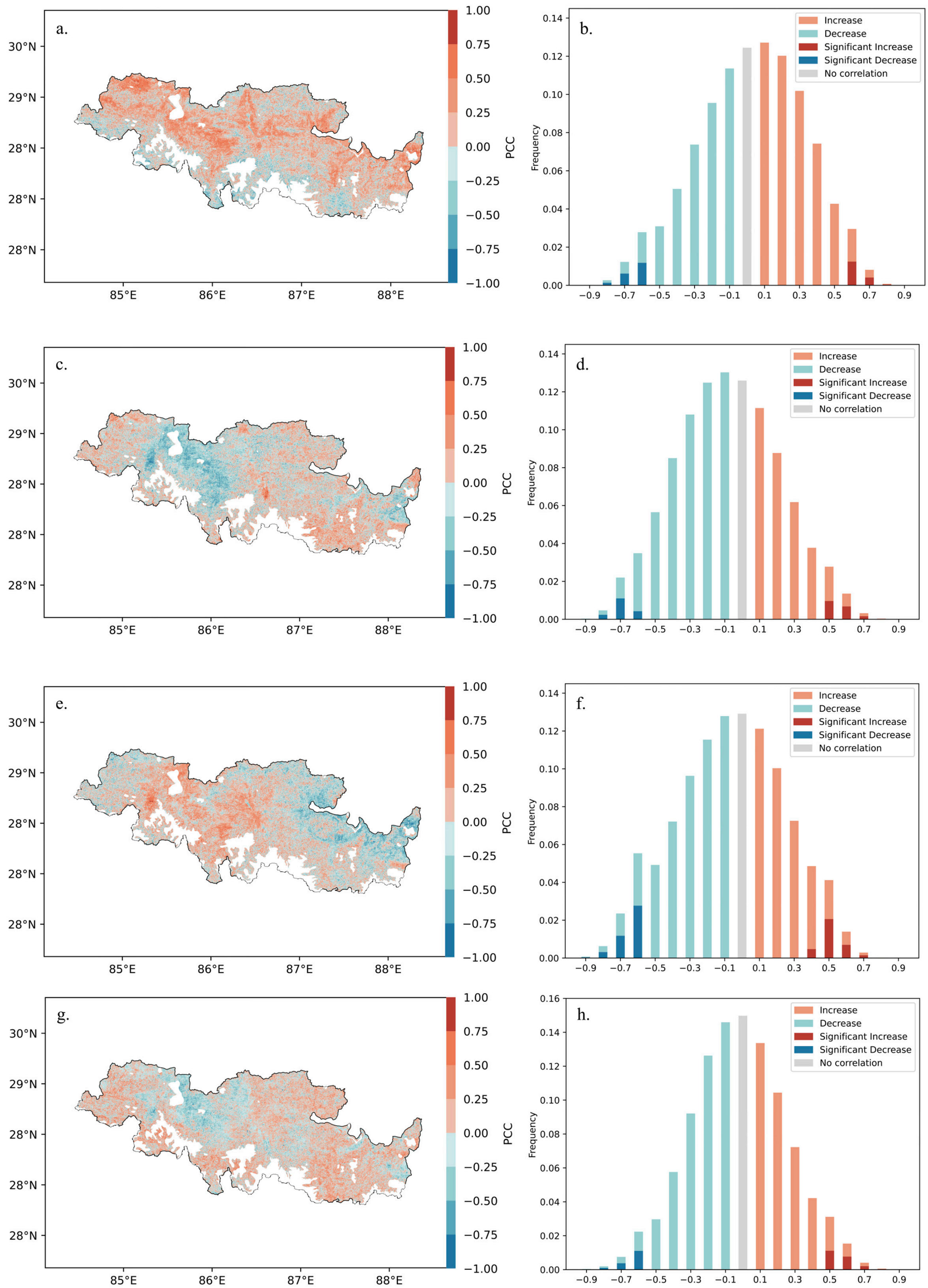

Figure 4. The partial correlation coefficient between the QNNR's growing season vegetation and hydrothermal parameters: (**a**) NDVI and precipitation; (**c**) NDVI and specific humidity; (**e**) NDVI and temperature; (**g**) NDVI and radiation. The frequency histogram of partial correlation level between the growing season vegetation and meteorological parameters: (**b**) NDVI and precipitation; (**d**) NDVI and specific humidity; (**f**) NDVI and temperature; (**h**) NDVI and radiation.

Figures 5 and 6 show the PLS-SEM results in 2000, 2005, 2010, and 2015. The evaluation findings of coefficient of predictive relevance (Q^2), goodness of fit (GOF), and determination (R^2) demonstrated that the PLS-SEM model performed well with a good capacity for explanatory power for the causal pathway (Table 4). Specifically, the NDVI's R2 fitted in an acceptable range. All variables had positive Stone–Geisser coefficients, indicating good predictive relevance regarding the endogenous latent variables. The path coefficients of PLE-SEM indicate that the interrelations between the latent variables were significant for all nine parameters ($p < 0.05$).

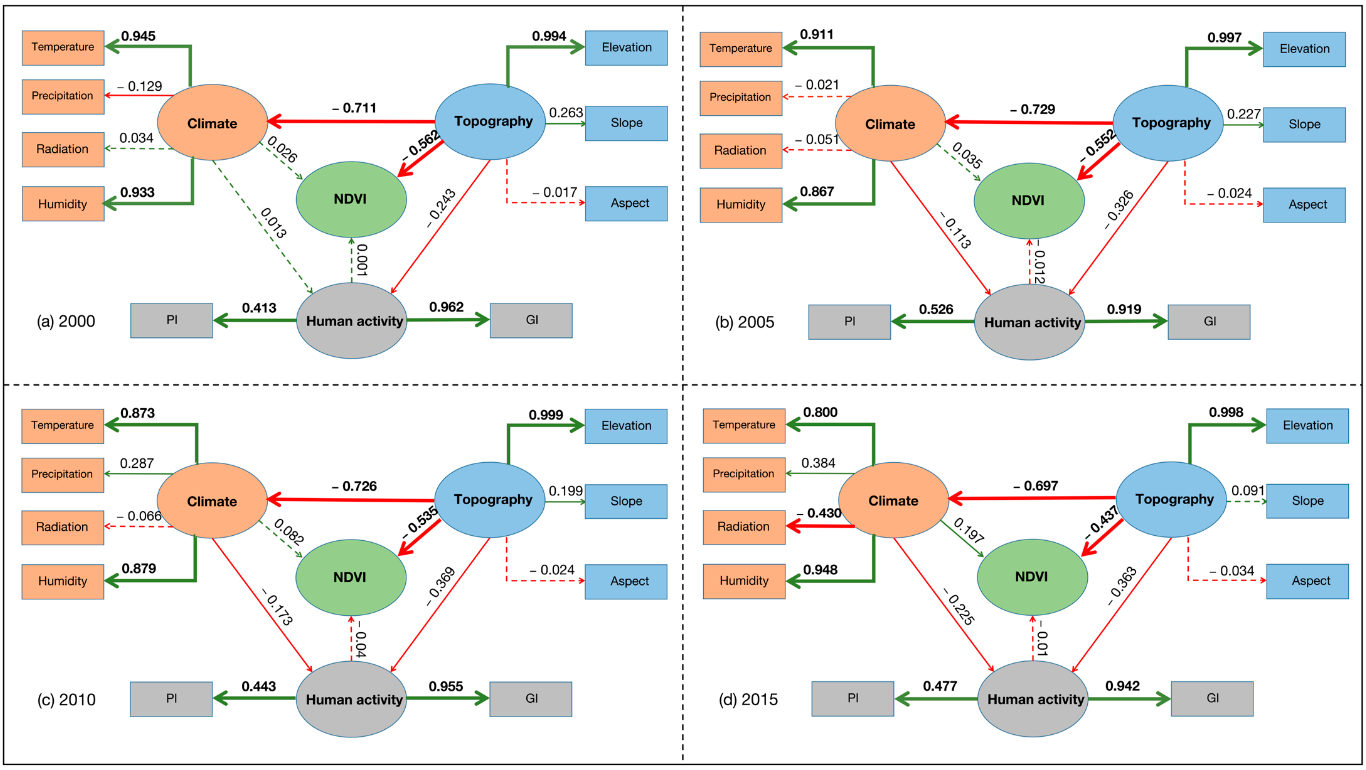

Figure 5. PLS-SEM for vegetation growth in the QNNR among climatic factors (temperature, precipitation, radiation, specific humidity), topographic factors (elevation, slope, aspect), and human activities (population intensity (PI), grazing intensity (GI)) in (**a**) 2000, (**b**) 2005, (**c**) 2010, and (**d**) 2015. The positive path coefficients are denoted by green arrows, whereas the negative path coefficients are denoted by red arrows. Bold lines show the absolute values of path coefficients greater than 0.4, thin lines show the absolute values of path coefficients between 0.1 and 0.4, and dashed lines show the absolute values of path coefficients less than 0.1.

Table 4. Assessment of the PLS-SEM.

Assessment Indicators	Types	Values			
		2000	2005	2010	2015
R2	NDVI	0.340	0.331	0.347	0.348
Q2	/	0.337	0.328	0.343	0.345
	Topographic factor →NDVI	0.000	0.000	0.000	0.000
p-value	Climatic factor → NDVI	0.000	0.000	0.000	0.000
	Human activity → NDVI	0.002	0.000	0.000	0.022
GOF	/	0.369	0.367	0.371	0.369

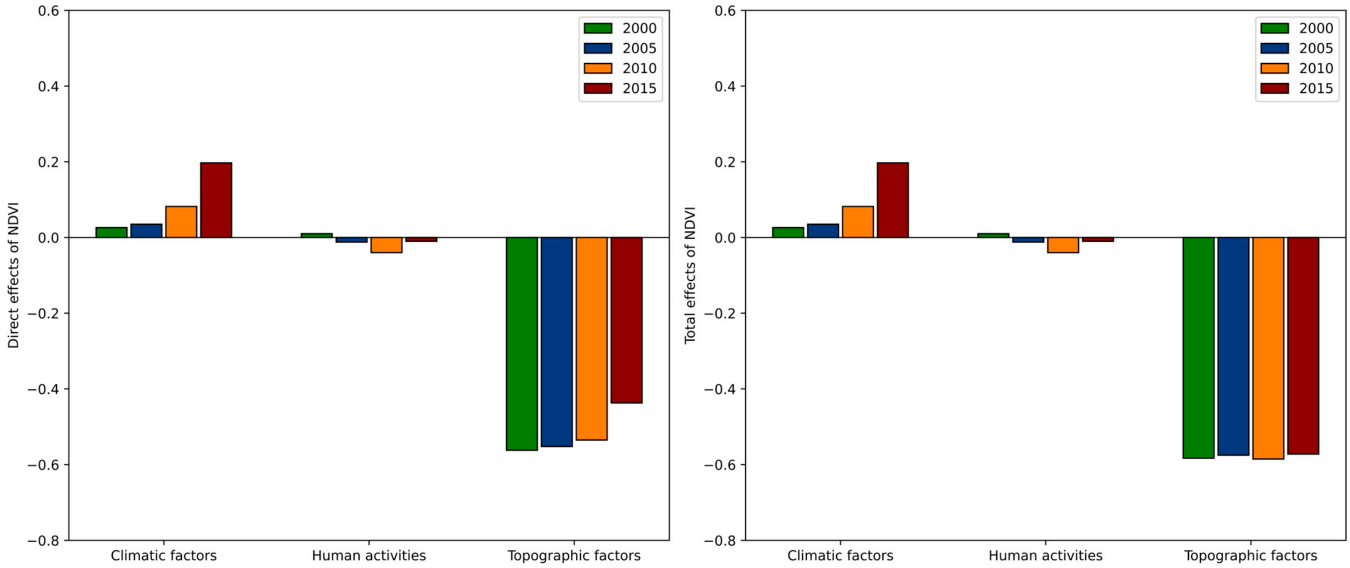

Figure 6. The direct effects and total effects of NDVI.

Among three latent variables (topographic, climatic, and artificial factors), topographic factors dominated the interpretation of NDVI, showing a downward trend of direct effects, an upward trend of indirect trend, and slight fluctuations of the total effects. In comparison, climatic factors' impact on NDVI was less, showing the increasing trends of both direct effect and total effect. Since human activity did not directly affect climate and topography in the established PLS-SEM model, the human activities' direct impact on vegetation was equal to its total effect that turned from positive to negative in 2010, which may be due to the implementation of local ecological programs. In terms of each latent variable, elevation was the most significant topographic element for the dynamics of vegetation, while slope and aspect had fewer positive impacts over the period. In terms of the four climatic factors, temperature and humidity had higher correlations with NDVI. Specifically, the effect of temperature decreased over the period, and that of humidity fluctuated slightly. The influence of precipitation changed from negative to positive, and became more and more positive over the years. In contrast, the effect of radiation turned from positive to increasingly negative. From the perspective of artificial factors, the impact of grazing on NDVI was much higher than that of human activity.

3.3.2. Uniform Manifold Approximation and Projection (UMAP)

The dimensionality reduction model based on the UMAP approach could effectively aggregate parameters by vegetation type. By combining the reduced model with different factors, the correlation between various vegetation types and variables could be derived (Figure 7). Specifically, elevation showed an obvious negative correlation with NDVI, while temperature was directly related to elevation. It can be observed from the scatter plot that the NDVI noticeably decreases when the temperature is below 5 °C and the elevation is more than 4000 m. The overall manifestation of human activity intensity was notably attenuated. Grazing intensity, mainly determined by vegetation types, was primarily distributed in the two largest clutters (grasslands and meadows). The vegetation types with high NDVI values were shrub and NF. While the NDVI values of meadow were controlled by elevation, showing a distinct changing pattern as the elevation gradient progressed. The variance in radiation is most conspicuous, with high radiation typically corresponding to low NDVI, and the highest radiation values were predominantly found in grasslands, meadows, and alpine vegetation. Even within a single type of vegetation, radiation exhibits significant heterogeneity, influenced by a combination of factors such as elevation, precipitation, and humidity. Furthermore, variations in humidity and precipitation usually occur in tandem.

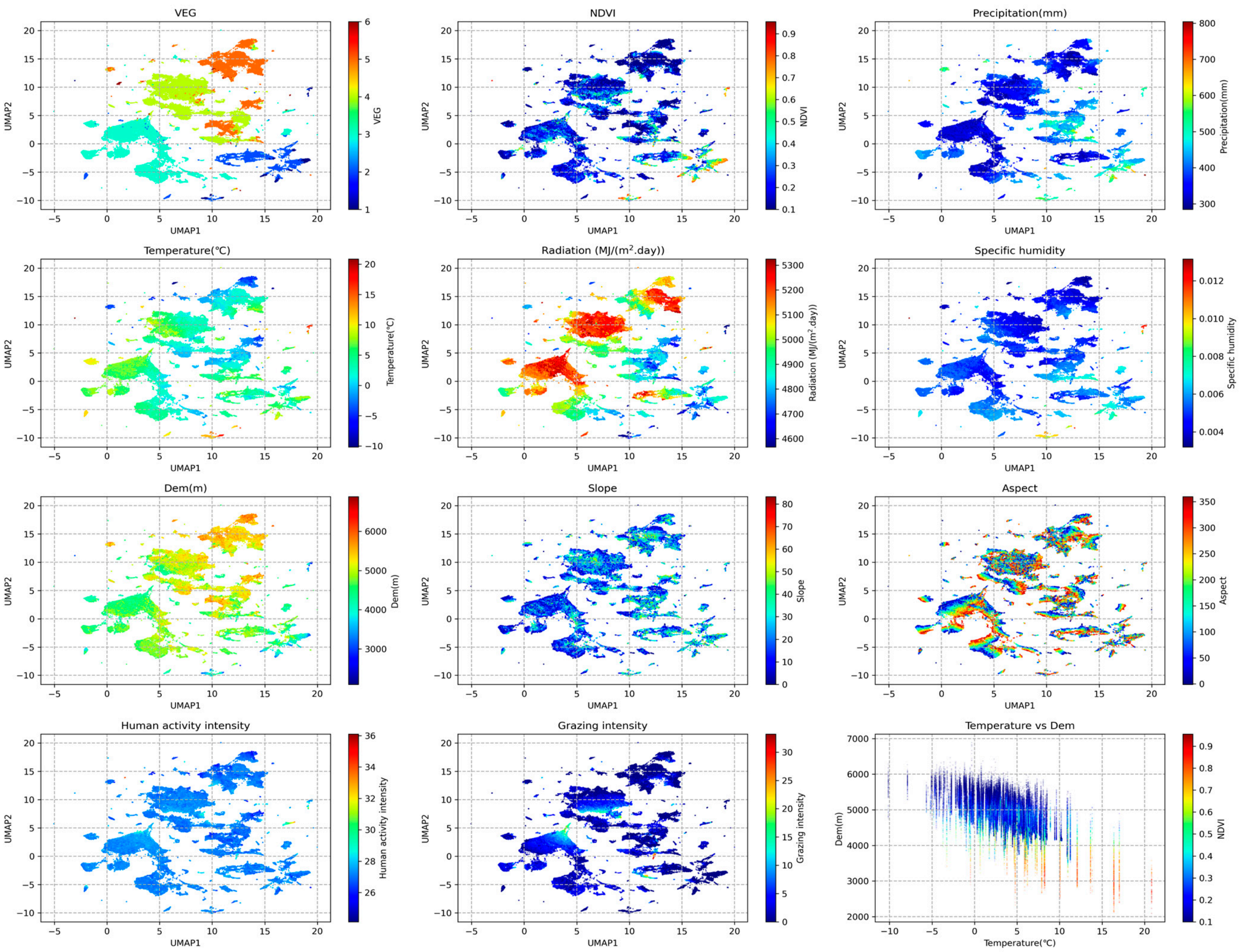

Figure 7. The comparative analysis of features using UMAP Dimensionality Reduction (vegetation type: 1—Needleleaf Forest (NF), 2—Shrub, 3—Grassland, 4—Meadow, 5—Alpine Vegetation (AV), 6—Cultural Vegetation (CV) (Each subplot indicated a two-dimensional projection in the UMAP space, with UMAP1 and UMAP2 as the primary axes. Individual points correspond to individual samples, with their color assigned based on the value of the specific feature denoted by each variable. The central distinction across these 11 subplots lies in the color assignment of the points, determined by different feature values. These features are specified in the title of each subplot. Within these subplots, points of analogous colors share proximity in the values of the respective feature. Consequently, a comparison across various subplots enables us to discern how specific features influence the distribution of samples within the two-dimensional space and carry out a comparative analysis). The lower right corner figure illustrated the interrelationships between temperature, elevation, and NDVI.

4. Discussion

4.1. The Spatiotemporal Trends of Vegetation and Its Partial Correlation with Meteorological Parameters

NDVI is frequently used to monitor vegetation's development and how it responds to climatic variation, because it is a reliable indication of plant growth status [89–91]. During the research period, the entire reserve displayed a growing season NDVI tendency of greening (0.0007/a) (Figure 3b), which was coincident with previous studies in the Everest area [92] and the QTP [93–98]. The NDVI interannual variance shifted from a decline to a noticeable increase in 2010 and continued to improve afterwards, which may be attributed to the execution of the Natural Forest Protection program, as well as to the improvements of hydrothermal conditions.

According to the NDVI trends, there was substantial geographic heterogenicity over the research period [99,100] (Figure 3b). The low temperature was identified in prior studies as one of the main barriers to vegetation coverage [101,102]. Due to the elevation-dependent warming (EDW) that occurs in mountainous places, the plateau warms more quickly than the plain areas [103–105], which significantly promotes vegetation growth in the plateau areas. Moreover, in the temperate alpine ecosystem, warm temperatures are also considered a major driving force behind seed germination, namely "the warm-cued germination", which increases the chance for plant survival during first-year establishment to withstand the cold winter on a plateau [12,106–110].

The PCC results (Figure 4e) showed that in the southwest and center of the reserve, the NDVI was positively associated with temperature, while the northeastern of the reserve contained the majority of the parts where vegetation negatively correlated with temperature. The northeastern part of the reserve experienced extremely low temperatures, which restricted the growth of vegetation to some extent. Even though there was a decreased tendency in precipitation over the study period, the drying had no discernible effects on the QNNR's vegetation development.

Based on the NDVI–precipitation partial correlations (Figure 4a), rainfall had a positive effect on vegetation development in the high-elevation regions of the north slope and a negative effect on NDVI in the south slope regions with more favorable hydrothermal conditions. However, in the areas with elevations ranging from 4200 to 4800 m, the north slope had a significantly lower NDVI value than the south slope, which had more heavy precipitation [111]. Because of the water stress effect on the northern slope, vegetation growth is more sensitive to precipitation [112], and with increasing elevation, precipitation decreases and soil water availability reduces, thereby limiting the dynamics of vegetation [113,114]. According to previous studies, the vegetation development may be constrained by the availability of water in mountainous, arid, and semi-arid locations [6,105,115–117]. The drying and warming would result in more soil moisture evaporation and less soil water availability in the reserve's north slope, where the elevation is higher [118,119]. This indicates how crucial precipitation and soil water availability are for the seedling establishment and vegetation dynamics in the reserve. The NDVI–radiation partial correlation (Figure 4g) revealed that greater radiation in the reserve's center inhibited the growth of vegetation. Changes in solar radiation brought on by clouds and aerosols primarily have an impact on vegetation growth by regulating how well plants absorb carbon dioxide [120]. Radiation also has an impact on turbulent surface energy flux, which is a contributing factor in evapotranspiration [120]. Thus, radiation influences vegetation transpiration and soil moisture constantly which would intensify the water stress effect on north slope areas and affect vegetation growth consequently. The comparatively low specific humidity in the QNNR's central region limits the growth of vegetation, which is probably because the lower humidity leads to the closure of some vegetation stomata affects the absorption of CO_2, and reduces photosynthesis (Figure 4c). Global warming caused the glaciers on Everest and its surroundings to thin at a pace of 0.38 0.04 m w.e./a between 2000 and 2012 AD [54,56,121–123]. This, to some extent, increased regional runoff and soil water, potentially reducing the impact of water stress in high-elevation locations.

4.2. Relationship between Vegetation Dynamics and Influencing Factors under the UMAP and PLS-SEM Analysis

Currently, it is commonly acknowledged that vegetation evolution is a complex process in which multiple factors work together, and research into the connection between vegetation dynamics and specific hydrothermal parameters is not rigorous enough [124–126]. The three main types of vegetation driving forces are (1) meteorological factors, which provide the fundamental conditions for vegetation development [127,128]; (2) topographic parameters which impact the vegetation development directly by themselves and also influence the distribution of climatic parameters that indirectly affect the spatial heterogeneity of vegetation coverage [129,130]; and (3) non-climatic disturbances resulting from human actions such as urban development, large construction projects, overgrazing, and deforestation [99,131].

The topography is a relatively constant factor in the context of global climate change and intensification of anthropogenic activity, and it merits investigation into how it influences vegetation growth both directly and indirectly, as well as how the distribution of vegetation responds to it. The PLS-SEM (Figure 5) and UMAP (Figure 7) results show that the main variables affecting NDVI are elevation, temperature, and humidity, with elevation being the most negatively correlated and temperature being most positively correlated with NDVI, especially in areas with high NDVI value. Humidity often reacts in tandem with precipitation. Anthropogenic factors are, to some extent, controlled by elevation. Two topographic factors, slope and aspect, indicate low correlations with NDVI and are not influenced by the differentiation of vegetation types. Previous studies have highlighted that the possible reason for slow vegetation development in the high-altitude regions of the QTP is the low nitrogen content that plays a major part in the development of photosynthetic organs such as chloroplasts, which concentrate around 75% of plant nitrogen [132,133]. Moreover, as elevation rises, the biomass of the leaf area, root nodules, mesophyll conductance, and stomatal declines noticeably, weakening the vegetation's capacity of absorbing nutrients and photosynthesis [134].

The results from our structural equation model showed that during the research period, elevation had adverse effects on vegetation development that were both direct and indirect (by influencing meteorological conditions). While the substantial elevational difference dominates the distribution of thermal conditions, the water vapor channel, which is likewise strongly correlated with elevation variation, has a considerable impact on the distribution of hydro conditions. Slope can influence vegetation growth by altering soil erosion rate, soil moisture, litter formation, and aspect, which can affect the vegetation's ability to photosynthesize [135].

However, as supported by the outcomes of other places in the QTP, our outcomes indicated that the effect of slope and aspect on vegetation in the QNNR is negligible in comparison to elevation [136]. The PLS-SEM findings also illustrated that the topographic variables, as a relatively constant indicator, demonstrated a decreasing direct effect on vegetation, whereas climatic elements steadily increased their influence on vegetation. This is partially attributable to the reserve's rising temperature trend during the research period, which somewhat overcomes the low-temperature restriction on vegetation development.

The melting of snow and glaciers brought on by warming reduces the water stress that results from increasing elevation, which also explains why the decreasing precipitation trend does not have a more detrimental effect on vegetation. This phenomenon lessens the negative effects of increasing elevation on vegetation. The greater association between specific humidity and NDVI in the PLS-SEM further illustrates how melting snow and glaciers raise humidity levels, which in turn leads to vegetation's stomata opening wider and absorbing more carbon dioxide, facilitating photosynthesis.

The increasing radiation accelerates vegetation transpiration, thus enhancing the water stress phenomenon and increasing the negative impact of radiation on vegetation. As not many people live in the reserve, human activates do not cause much environmental harm, despite the fact that they are intensifying. According to the structural equation model, human activity positively affected vegetation in 2000, demonstrating the benefits of modest grazing [35,137]. Light and moderate grazing activity both have a positive effect on vegetation diversification and soil respiration in the grassland ecosystems of the QTP, where vegetation covering, above-ground biomass, total nitrogen, and SOC exhibit a slight linear development connection with grazing intensity [138].

Unfortunately, human activities negatively influenced the growth of vegetation in the reserve in 2005 and 2010 due to the expansion of urban areas. To reduce the damages caused by human activities, several ecological policies including prohibiting grazing and offering reward-compensation mechanisms for herdsmen [139] were implemented by the local government. Thus, the regional livestock growth trend reversed from an increase to a decrease around 2009, with a sharp decline since 2010. Our PLS-SEM findings demonstrate that the detrimental influence of human activity peaked in 2010 and then declined in 2015, highlighting the contribution of ecological policies [51,140–143]. In conclusion, topographic factors, followed by climatic elements, have the most power over the growth of vegetation in the QNNR, whereas anthropogenic causes have the smallest impact.

4.3. Limitations and Prospects

This study analyzed the variations in vegetation development and hydrothermal parameters, and it qualified the influences of topography, hydrothermal conditions, and human activity on vegetation growth in the reserve. The limitations of this paper are as follows: (1) Limited by only two meteorological stations located in the reserve, the ground-observed data is insufficient for interpolation, and the coarse spatial resolution of CMFD affects the partial correlation calculation. (2) The model only considered four hydrometeorological factors, three topographic factors, and two anthropogenic activity indicators; the structural equation model fitting is still limited. In further studies, more auxiliary data is necessary to generate more precise climatic raster data. Moreover, to more precisely evaluate the influence of natural and artificial variables on vegetation cover in the reserve, additional indicators, such as water cycle, evaporation, population, and land use, might be extensively taken into consideration in PLS-SEM. (3) Over the last few decades, a variety of remote sensing vegetation indices have been developed, such as the Normalized Difference Vegetation Index (NDVI), Global Environmental Monitoring Index (GEMI), Difference Vegetation Index (DVI), Simple Ratio Vegetation Index (SR), Soil-Adjusted Vegetation Index (SAVI), Enhanced Vegetation Index (EVI), Aerosol Free Vegetation Index (AFVI), and the Medium Resolution Imaging Spectrometer Terrestrial Chlorophyll Index (MTCI). Although NDVI is deemed sufficient for the scope of this study, other indices might be employed in the future to obtain a more holistic and comprehensive assessment of regional vegetation dynamics.

5. Conclusions

From 2000 to 2018, the entire reserve exhibited an improving trend in vegetation at a rate of 0.0007/a, exceeding the typical levels of the Qinghai–Tibet Plateau. The partial correlation analysis indicated substantial spatial heterogeneity between the growing season NDVI and hydrothermal parameters, with different impacts of hydrothermal factors on the vegetation development of the northern and southern slopes, suggesting that water stress could potentially influence vegetation growth to some extent. Moreover, the vegetation response to meteorological factors displayed a certain correlation with elevation; specifically, a noticeable decrease in NDVI occurred when the temperature was below 5 °C and elevation exceeded 4000 m. The PLS-SEM results suggested that for the vegetation development in the QNNR, topographic factors, particularly elevation, played a dominant role, while the influence of climatic factors gradually increased over each five-year period, with relatively rare impacts from anthropogenic activities. Therefore, the natural environment in the QNNR has benefited from the implementation of ecological programs. Visualization through the UMAP approach revealed a distinct negative correlation between elevation and NDVI, with temperature directly associated with elevation. The overall manifestation of human activity intensity was notably attenuated, and grazing intensity was mainly determined by vegetation types, predominantly distributed within the two largest clusters (grasslands and meadows).

Author Contributions: Conceptualization, B.X., J.L. and P.P.; methodology, B.X. and T.Z.; software, B.X. and G.Y.; validation, B.X. and X.B.; formal analysis, B.X. and X.B.; investigation, L.B.; resources, X.P.; data curation, B.X. and L.B.; writing—original draft preparation, B.X. and J.L.; writing—review and editing, B.X. and J.L.; visualization, B.X., J.L. and G.Y.; supervision, J.L. and X.P.; project administration, J.L. and P.P.; funding acquisition, J.L. All authors have read and agreed to the published version of the manuscript.

Funding: This research was funded by the Second Tibetan Plateau Scientific Expedition and Research Program (STEP) (Grant No. 2019QZKK0307), and the National Natural Science Foundation of China (41501060).

Data Availability Statement: Data available on request from the authors.

Acknowledgments: We are grateful to NASA (https://ladsweb.modaps.eosdis.nasa.gov/ accessed on 5 February 2023), National Tibetan Plateau Data Center (http://data.tpdc.ac.cn/ accessed on 7 February 2023), Resource and Environment Science and Data Center (https://www.resdc.cn/ accessed on 8 February 2023), Geospatial Data Cloud (https://www.gscloud.cn/ accessed on 8 February 2023)for providing data.

Conflicts of Interest: The authors declare no conflict of interest.

References

1. Zhang, X.; Liao, C.; Li, J.; Sun, Q. Fractional vegetation cover estimation in arid and semi-arid environments using HJ-1 satellite hyperspectral data. *Int. J. Appl. Earth Obs. Geoinf.* **2013**, *21*, 506–512. [CrossRef]
2. Song, W.; Mu, X.; Ruan, G.; Gao, Z.; Li, L.; Yan, G. Estimating fractional vegetation cover and the vegetation index of bare soil and highly dense vegetation with a physically based method. *Int. J. Appl. Earth Obs. Geoinf.* **2017**, *58*, 168–176. [CrossRef]
3. Hu, Y.F.; Dao, R.N.; Hu, Y. Vegetation Change and Driving Factors: Contribution Analysis in the Loess Plateau of China during 2000–2015. *Sustainability* **2019**, *11*, 1320. [CrossRef]
4. Ning, T.T.; Liu, W.Z.; Lin, W.; Song, X.Q.; Mischke, S. NDVI Variation and Its Responses to Climate Change on the Northern Loess Plateau of China from 1998 to 2012. *Adv. Meteorol.* **2015**, *2015*, 1–10. [CrossRef]
5. Chen, T.; Xia, J.; Zou, L.; Hong, S. Quantifying the Influences of Natural Factors and Human Activities on NDVI Changes in the Hanjiang River Basin, China. *Remote Sens.* **2020**, *12*, 3780. [CrossRef]
6. Nemani, R.R.; Keeling, C.D.; Hashimoto, H.; Jolly, W.M.; Piper, S.C.; Tucker, C.J.; Myneni, R.B.; Running, S.W. Climate-driven increases in global terrestrial net primary production from 1982 to 1999. *Science* **2003**, *300*, 1560–1563. [CrossRef]
7. Zhao, X.; Tan, K.; Zhao, S.Q.; Fang, J. Changing climate affects vegetation growth in the arid region of the Northwestern China. *J. Arid Environ.* **2011**, *75*, 946–952. [CrossRef]
8. Peñuelas, J.; Ogaya, R.; Boada, M.; Jump, A.S. Migration, invasion and decline: Changes in recruitment and forest structure in a warming-linked shift of European beech forest in Catalonia (NE Spain). *Ecography* **2007**, *30*, 829–837. [CrossRef]
9. Piao, S.; Wang, X.; Park, T.; Chen, C.; Lian, X.; He, Y.; Bjerke, J.W.; Chen, A.; Ciais, P.; Tømmervik, H.; et al. Characteristics, drivers and feedbacks of global greening. *Nat. Rev. Earth Environ.* **2020**, *1*, 14–27. [CrossRef]
10. Lenoir, J.; Gégout, J.; Marquet, P.; De Ruffray, P.; Brisse, H. A significant upward shift in plant species optimum elevation during the 20th century. *Science* **2008**, *320*, 1768–1771. [CrossRef]
11. Zhang, Y.L.; Gao, J.G.; Liu, L.S.; Wang, Z.F.; Ding, M.J.; Yang, X.C. NDVI-based vegetation changes and their responses to climate change from 1982 to 2011, A case study in the Koshi river basin in the middle Himalayas. *Glob. Planet. Chang.* **2013**, *108*, 139–148. [CrossRef]
12. Li, L.; Zhang, Y.; Liu, L.; Wu, J.; Wang, Z.; Li, S.; Zhang, H.; Zu, J.; Ding, M.; Paudel, B. Spatiotemporal patterns of vegetation greenness change and associated climatic and anthropogenic drivers on the Tibetan Plateau during 2000–2015. *Remote Sens.* **2018**, *10*, 1525. [CrossRef]
13. Kim, Y.; Kimball, J.S.; Zhang, K.; McDonald, K.C. Satellite detection of increasing northern hemisphere non-frozen seasons from 1979 to 2008, Implications for regional vegetation growth. *Remote Sens. Environ.* **2012**, *121*, 472–487. [CrossRef]
14. Sun, W.C.; Wang, Y.Y.; Fu, Y.H.; Xue, B.L.; Wang, G.Q.; Yu, J.S.; Zuo, D.P.; Xu, Z.X. Spatial heterogeneity of changes in vegetation growth and their driving forces based on satellite observations of the Yarlung Zangbo River basin in the Tibetan plateau. *J. Hydrol.* **2019**, *574*, 324–332. [CrossRef]
15. Seddon, A.W.; Macias-Fauria, M.; Long, P.R.; Benz, D.; Willis, K.J. Sensitivity of global terrestrial ecosystems to climate variability. *Nature* **2016**, *531*, 229–244. [CrossRef]
16. Wang, B.; Zhang, G.; Duan, J. Relationship between topography and the distribution of understory vegetation in a Pinus massoniana forest in Southern China. *Int. Soil Water Conserv. Res.* **2015**, *3*, 291–304. [CrossRef]
17. Riihimäki, H.; Heiskanen, J.; Luoto, M. The effect of topography on arctic-alpine aboveground biomass and NDVI patterns. *Int. J. Appl. Earth Obs. Geoinf.* **2017**, *56*, 44–53. [CrossRef]
18. Liu, C.; Li, W.; Wang, W.; Zhou, H.; Liang, T.; Hou, F.; Xu, J.; Xue, P. Quantitative spatial analysis of vegetation dynamics and potential driving factors in a typical alpine region on the northeastern Tibetan Plateau using the Google Earth Engine. *Catena* **2021**, *206*, 105500. [CrossRef]
19. Liang, L.; Wang, Q.; Guan, Q.; Du, Q.; Sun, Y.; Ni, F.; Lv, S.; Shan, Y. Assessing vegetation restoration prospects under different environmental elements in cold and arid mountainous region of China. *Catena* **2023**, *226*, 107055. [CrossRef]
20. Holtmeier, F.; Broll, G. Sensitivity and response of northern hemisphere altitudinal and polar treelines to environmental change at landscape and local scales. *Glob. Ecol. Biogeogr.* **2005**, *14*, 395–410. [CrossRef]

21. Körner, C. *Alpine Treelines: Functional Ecology of the Global High Elevation Tree Limits*; Springer Science and Business Media: Berlin/Heidelberg, Germany, 2012. [CrossRef]
22. Zhang, Y.; He, N.; Liu, Y. Temperature factors are a primary driver of the forest bryophyte diversity and distribution in the southeast Qinghai-Tibet Plateau. *For. Ecol. Manag.* **2023**, *527*, 120610. [CrossRef]
23. Sun, J.; Cheng, G.; Li, W.; Sha, Y.; Yang, Y. On the variation of NDVI with the principal climatic elements in the Tibetan Plateau. *Remote Sens.* **2013**, *5*, 1894–1911. [CrossRef]
24. Shi, Y.; Wang, Y.; Ma, Y.; Ma, W.; Liang, C.; Flynn, D.; Schmid, B.; Fang, J.; He, J. Field-based observations of regional-scale, temporal variation in net primary production in Tibetan alpine grasslands. *Biogeosciences* **2014**, *11*, 2003–2016. [CrossRef]
25. Pang, G.; Wang, X.; Yang, M. Using the NDVI to identify variations in, and responses of, vegetation to climate change on the Tibetan Plateau from 1982 to 2012. *Quat. Int.* **2017**, *444*, 87–96. [CrossRef]
26. Piao, S.; Fang, J.; Zhou, L.; Guo, Q.; Henderson, M.; Ji, W.; Li, Y.; Tao, S. Interannual variations of monthly and seasonal normalized difference vegetation index (NDVI) in China from 1982 to 1999. *J. Geophys. Res.* **2003**, *108*, 4401. [CrossRef]
27. Liu, S.; Zhang, Y.; Cheng, F.; Hou, X.; Zhao, S. Response of grassland degradation to drought at different time-scales in Qinghai Province: Spatio-temporal characteristics, correlation, and implications. *Remote Sens.* **2017**, *9*, 1329. [CrossRef]
28. Kennedy, C.M.; Oakleaf, J.R.; Theobald, D.M.; Baruch-Mordo, S.; Kiesecker, J. Managing the middle: A shift in conservation priorities based on the global human modification gradient. *Glob. Chang. Biol.* **2019**, *25*, 811–826. [CrossRef]
29. Shen, Q.; Gao, G.; Han, F.; Xiao, F.; Ma, Y.; Wang, S.; Fu, B. Quantifying the effects of human activities and climate variability on vegetation cover change in a hyper-arid endorheic basin. *Land Degrad. Dev.* **2018**, *29*, 3294–3304. [CrossRef]
30. Wang, F.T.; An, P.L.; Huang, C.; Zhang, Z.; Hao, J.M. Is afforestation-induced land use change the main contributor to vegetation dynamics in the semiarid region of North China? *Ecol. Indic.* **2018**, *88*, 282–291. [CrossRef]
31. Fang, W.; Huang, S.Z.; Huang, Q.; Huang, G.H.; Wang, H.; Leng, G.Y.; Wang, L.; Guo, Y. Probabilistic assessment of remote sensing-based terrestrial vegetation vulnerability to drought stress of the Loess Plateau in China. *Remote Sens. Environ.* **2019**, *232*, 111290. [CrossRef]
32. Duan, W.L.; Zou, S.; Chen, Y.N.; Daniel, N.; Fang, G.H.; Wang, Y. Sustainable water management for cross-border resources: The Balkhash Lake Basin of Central Asia, 1931–2015. *J. Clean. Prod.* **2020**, *263*, 121614. [CrossRef]
33. Guillermo, G.; Julio, C.J.; Raúl, S.-S.; Navarro, C.R.M. Limited Growth Recovery after Drought-Induced Forest Dieback in Very Defoliated Trees of Two Pine Species. *Front. Plant Sci.* **2016**, *7*, 418. [CrossRef]
34. Ma, J.N.; Zhang, C.; Guo, H.; Chen, W.L.; Yun, W.J.; Gao, L.L.; Wang, H. Analyzing Ecological Vulnerability and Vegetation Phenology Response Using NDVI Time Series Data and the BFAST Algorithm. *Remote Sens.* **2020**, *12*, 3371. [CrossRef]
35. Dong, S.; Shang, Z.; Gao, J.; Boone, R.B. Enhancing sustainability of grassland ecosystems through ecological restoration and grazing management in an era of climate change on Qinghai-Tibetan Plateau. *Agric. Ecosyst. Environ.* **2020**, *287*, 106684. [CrossRef]
36. Liu, J.; Milne, R.I.; Cadotte, M.W.; Wu, Z.Y.; Provan, J.; Zhu, G.F.; Gao, L.M.; Li, D.Z. Protect Third Pole's fragile ecosystem. *Science* **2018**, *362*, 1368. [CrossRef]
37. Harris, R.B. Rangeland degradation on the Qinghai-Tibetan plateau: A review of the evidence of its magnitude and causes. *J. Arid Environ.* **2010**, *74*, 1–12. [CrossRef]
38. Piao, S.; Yin, G.; Tan, J.; Cheng, L.; Huang, M.; Li, Y.; Liu, R.; Mao, J.; Myneni, R.B.; Peng, S. Detection and attribution of vegetation greening trend in China over the last 30 years. *Glob. Chang. Biol.* **2015**, *21*, 1601–1609. [CrossRef]
39. Mishra, N.B.; Mainali, K.P. Greening and browning of the Himalaya: Spatial patterns and the role of climatic change and human drivers. *Sci. Total Environ.* **2017**, *587*, 326–339. [CrossRef]
40. Huang, W.J.; Duan, W.L.; Chen, Y.N. Rapidly declining surface and terrestrial water resources in Central Asia driven by socio-economic and climatic changes. *Sci. Total Environ.* **2021**, *784*, 147193. [CrossRef]
41. Yao, T.D.; Thompson, L.; Yang, W.; Yu, W.S.; Gao, Y.; Guo, X.J.; Yang, X.X.; Duan, K.Q.; Zhao, H.B.; Xu, B.Q.; et al. Different glacier status with atmospheric circulations in Tibetan Plateau and surroundings. *Nat. Clim. Chang.* **2012**, *2*, 663–667. [CrossRef]
42. Immerzeel, W.W.; van Beek, L.P.H.; Bierkens, M.F.P. Climate change will affect the Asian water towers. *Science* **2010**, *328*, 1382–1385. [CrossRef]
43. An, Z.; Wu, G.; Li, J.; Sun, Y.; Liu, Y.; Zhou, W.; Cai, Y.; Duan, A.; Li, L.; Mao, J. Global monsoon dynamics and climate change. Annu. *Rev. Earth Planet. Sci.* **2015**, *43*, 29–77. [CrossRef]
44. Li, Y.; Ding, Y.; Li, W. Interdecadal variability of the Afro-Asian summer monsoon system. *Adv. Atmos. Sci.* **2017**, *34*, 833–846. [CrossRef]
45. Li, J.; Zheng, F.; Sun, C.; Feng, J.; Wang, J. Pathways of influence of the Northern Hemisphere mid-high latitudes on East Asian climate: A review. *Adv. Atmos. Sci.* **2019**, *36*, 902–921. [CrossRef]
46. Dolezal, J.; Dvorsky, M.; Kopecky, M.; Liancourt, P.; Hiiesalu, I.; Macek, M.; Altman, J.; Chlumska, Z.; Rehakova, K.; Capkova, K.; et al. Vegetation dynamics at the upper elevational limit of vascular plants in Himalaya. *Sci. Rep.* **2016**, *6*, 24881. [CrossRef]
47. Mayewski, P.A.; Perry, L.B.; Matthews, T.; Birkel, S.D. Climate change in the Hindu Kush Himalayas: Basis and Gaps. *One Earth* **2020**, *3*, 551–555. [CrossRef]
48. Zhu, C. General Situation of Mt. Qomolangma Natural Reservoir. *China Tibetol.* **1997**, *1*, 3–22. (In Chinese)
49. Zhang, D.; Huang, J.; Guan, X.; Chen, B.; Zhang, L. Long-term trends of precipitable water and precipitation over the Tibetan Plateau derived from satellite and surface measurements. *J. Quant. Spectrosc. Radiat. Transf.* **2013**, *122*, 64–71. [CrossRef]

50. Pachauri, R.K.; Allen, M.R.; Barros, V.R.; Broome, J.; Cramer, W.; Christ, R.; Church, J.A.; Clarke, L.; Dahe, Q.; Dasgupta, P.; et al. *Climate Change 2014, Synthesis Report. Contribution of Working Groups I, II and III to the Fifth Assessment Report of the Intergovernmental Panel on Climate Change*; IPCC: Geneva, Switzerland, 2014; 151p, ISBN 978-92-9169-143-2.
51. Li, S.; Wu, J.; Gong, J.; Li, S. Human footprint in Tibet: Assessing the spatial layout and effectiveness of nature reserves. *Sci. Total Environ.* **2018**, *621*, 18–29. [CrossRef]
52. Peng, S.; Piao, S.; Ciais, P.; Fang, J.; Wang, X. Change in winter snow depth and its impacts on vegetation in China. *Glob. Chang. Biol.* **2010**, *16*, 3004–3013. [CrossRef]
53. Bolch, T.; Shea, J.M.; Liu, S.; Azam, F.M.; Gao, Y.; Gruber, S.; Immerzeel, W.W.; Kulkarni, A.; Li, H.; Tahir, A.A.; et al. Status and change of the cryosphere in the extended Hindu Kush Himalaya region. In *The Hindu Kush Himalaya Assessment: Mountains, Climate Change, Sustainability and People*; Wester, P., Mishra, A., Mukherji, A., Shrestha, B., Eds.; Springer International Publishing: Cham, Switzerland, 2019; pp. 209–255.
54. Liu, S.; Yao, X.; Guo, W.; Xu, J.; Shangguan, D.; Wei, J.; Bao, W.; Wu, L. The contemporary glaciers in China based on the Second Chinese Glacier Inventory. *Acta Geograph. Sin.* **2015**, *70*, 3–16. [CrossRef]
55. Ye, Q.; Bolch, T.; Naruse, R.; Wang, Y.; Zong, J.; Wang, Z.; Zhao, R.; Yang, D.; Kang, S. Glacier mass changes in Rongbuk catchment on Mt. Qomolangma from 1974 to 2006 based on topographic maps and ALOS PRISM data. *J. Hydrol.* **2015**, *530*, 273–280. [CrossRef]
56. Guo, W.; Liu, S.; Xu, L.; Wu, L.; Shangguan, D.; Yao, X.; Wei, J.; Bao, W.; Yu, P.; Liu, Q.; et al. The second Chinese glacier inventory: Data, methods and results. *J. Glaciol.* **2015**, *61*, 357–372. [CrossRef]
57. Zhang, B.; Zhang, Y.; Wang, Z.; Ding, M.; Liu, L.; Li, L.; Li, S.; Liu, Q.; Paudel, B.; Zhang, H. Factors Driving Changes in Vegetation in Mt. Qomolangma (Everest): Implications for the Management of Protected Areas. *Remote Sens.* **2021**, *13*, 4725. [CrossRef]
58. Ma, F.; Peng, P. Spatial-temporal dynamics of alpine grassland coverage and its response to climate warming in Mt. Qomolangma Nature Preserve during 2000–2019. *J. Mt. Sci.* **2022**, *19*, 2297–2311. [CrossRef]
59. Tan, J.; Piao, S.; Chen, A.; Zeng, Z.; Ciais, P.; Janssens, I.A.; Mao, J.; Myneni, R.B.; Peng, S.; Peñuelas, J.; et al. Seasonally different response of photosynthetic activity to daytime and night-time warming in the northern hemisphere. *Glob. Chang. Biol.* **2015**, *21*, 377–387. [CrossRef]
60. Chen, L.; Hänninen, H.; Rossi, S.; Smith, N.G.; Pau, S.; Liu, Z.; Feng, G.; Gao, J.; Liu, J. Leaf senescence exhibits stronger climatic responses during warm than during cold autumns. *Nat. Clim. Chang.* **2020**, *10*, 777–780. [CrossRef]
61. Parente, A.; Sutherland, J.C. Principal component analysis of turbulent combustion data: Data pre-processing and manifold sensitivity. *Combust. Flame* **2013**, *160*, 340–350. [CrossRef]
62. Wang, S.J.; Tang, X.Y.; Wang, G.; Li, Y.Q. Study on the climatic characteristics in the mount Qomolangma region during the last 53 Years. *Plateau Mt. Meteorol. Res.* **2021**, *41*, 2–6. [CrossRef]
63. Kang, S.C.; Zhang, Q.G.; Zhang, Y.L.; Guo, W.Q.; Ji, Z.M.; Shen, M.; Wang, S.; Wang, X.; Tripathee, L.; Liu, Y.; et al. Warming and thawing in the Mt. Everest region: A review of climate and environmental changes. *Earth-Sci. Rev.* **2022**, *225*, 103911. [CrossRef]
64. Liu, Z.; Wang, H.; Li, N.; Zhu, J.; Pan, Z.; Qin, F. Spatial and Temporal Characteristics and Driving Forces of Vegetation Changes in the Huaihe River Basin from 2003 to 2018. *Sustainability* **2020**, *12*, 2198. [CrossRef]
65. Yang, K.; He, J.; Tang, W.; Lu, H.; Qin, J.; Chen, Y.; Li, X. China meteorological forcing dataset (1979–2018). In *A Big Earth Data Platform for Three Poles*; National Tibetan Plateau Data Center: Beijing, China, 2019. [CrossRef]
66. He, J.; Yang, K.; Tang, W.; Lu, H.; Qin, J.; Chen, Y.Y.; Li, X. The first high-resolution meteorological forcing dataset for land process studies over China. *Sci. Data* **2020**, *7*, 25. [CrossRef]
67. Liu, S.; Sun, Y.; Liu, Y.; Li, M. *1 km Grid Datasets of Human Activity Intensity in Agricultural and Pastoral Areas of the Qinghai-Tibet Plateau (1990–2015)*; National Tibetan Plateau Data Center: Beijing, China, 2023. [CrossRef]
68. Sen, P.K. Estimates of the regression coefficient based on Kendall's Tau. *J. Am. Stat. Assoc.* **1968**, *63*, 1379–1389. [CrossRef]
69. Kendall, M. *Rank Correlation Methods*; Charles Griffin & Co. Ltd.: London, UK, 1975.
70. Kalisa, W.; Igbawua, T.; Henchiri, M.; Ali, S.; Zhang, S.; Bai, Y.; Zhang, J. Assessment of climate impact on vegetation dynamics over East Africa from 1982 to 2015. *Sci. Rep.* **2019**, *9*, 16865. [CrossRef]
71. Sun, H.; Wang, C.; Niu, Z. Analysis of the vegetation cover change and the relationship between NDVI and environmental factors by using NOAA time series data. *J. Remote Sens.* **1998**, *2*, 210–216. [CrossRef]
72. Hair, J.F.; Sarstedt, M.; Hopkins, L.G.; Kuppelwieser, V. Partial least squares structural equation modeling (PLS-SEM): An emerging tool in business research. *Eur. Bus. Rev.* **2014**, *26*, 106–121. [CrossRef]
73. Pearl, J. The causal mediation formula-a guide to the assessment of pathways and mechanisms. *Prev. Sci.* **2012**, *13*, 426–436. [CrossRef] [PubMed]
74. Hair, J.F.; Ringle, C.M.; Sarstedt, M. PLS-SEM: Indeed a silver bullet. *J. Mark. Theory Pract.* **2011**, *19*, 139–152. [CrossRef]
75. Hair, J.F.; Sarstedt, M.; Ringle, C.M.; Mena, J.A. An assessment of the use of partial least squares structural equation modeling in marketing research. *J. Acad. Mark. Sci.* **2012**, *40*, 414–433. [CrossRef]
76. Vinzi, V.E.; Trinchera, L.; Amato, S. PLS path modeling: From foundations to recent developments and open issues for model assessment and improvement. In *Handbook of Partial Least Squares*; Springer: Berlin/Heidelberg, Germany, 2010; pp. 47–82. [CrossRef]
77. Hayes, A.F. Beyond Baron and Kenny: Statistical mediation analysis in the new millennium. *Commun. Monogr.* **2009**, *76*, 408–420. [CrossRef]

78. Chin, W.W. The partial least squares approach to structural equation modeling. *Mod. Methods Bus. Res.* **1998**, *295*, 295–336.
79. Stone, M. Cross-validatory choice and assessment of statistical predictions. *J. R. Stat. Soc. Ser. B (Methodol.)* **1974**, *36*, 111–133. [CrossRef]
80. Tenenhaus, M.; Amato, S.; Esposito Vinzi, V. A global goodness-of-fit index for PLS structural equation modelling. *Proc. XLII SIS Sci. Meet.* **2004**, *1*, 739–742.
81. Clarke, R.; Ressom, H.; Wang, A.; Xuan, J.; Liu, M.C.; Gehan, E.A.; Wang, Y. The properties of high-dimensional data spaces: Implications for exploring gene and protein expression data. *Nat. Rev. Cancer* **2008**, *8*, 37–49. [CrossRef] [PubMed]
82. Altman, N.; Krzywinski, M. The curse(s) of dimensionality. *Nat. Methods* **2018**, *15*, 399–400. [CrossRef]
83. Egger, R. *Applied Data Science in Tourism: Interdisciplinary Approaches, Methodologies, and Applications*; Springer Nature Switzerland AG: Cham, Switzerland, 2021; pp. 2366–2611. [CrossRef]
84. Ringnér, M. What is principal component analysis? *Nat. Biotechnol.* **2008**, *26*, 303–304. [CrossRef] [PubMed]
85. Mahmoudi, M.R.; Heydari, M.H.; Qasem, S.N.; Mosavi, A.; Band, S.S. Principal component analysis to study the relations between the spread rates of COVID-19 in high risks countries. *Alexandria Eng. J.* **2021**, *60*, 457–464. [CrossRef]
86. Maaten, L.v.d.; Hinton, G. Visualizing data using t-sne. *J. Mach. Learn Res.* **2008**, *9*, 2579–2605.
87. McInnes, L.; Healy, J.; Melville, J. UMAP: Uniform manifold approximation and projection for dimension reduction. *J. Open Source Softw.* **2018**, *3*, 861. [CrossRef]
88. Legendre, P.; Gallagher, E.D. Ecologically meaningful transformations for ordination of species data. *Oecologia* **2001**, *129*, 271–280. [CrossRef]
89. Myer-Smith, I.H.; Kerby, J.T.; Phoenix, G.K.; Bjerke, J.W.; Epstein, H.E.; Assmann, J.J.; John, C.; Andreu-Hayles, L.; Angers-Blondin, S.; Beck, P.S.A.; et al. Complexity revealed in the greening of the Arctic. *Nat. Clim. Chang.* **2020**, *10*, 106–117. [CrossRef]
90. Piao, S.; Nan, H.; Huntingford, C.; Ciais, P.; Friedlingstein, P.; Sitch, S.; Chen, A. Evidence for a weakening relationship between interannual temperature variability and northern vegetation activity. *Nat. Commun.* **2014**, *5*, 5018. [CrossRef] [PubMed]
91. Shen, M.; Piao, S.; Cong, N.; Zhang, G.; Janssens, I.A. Precipitation impacts on vegetation spring phenology on the Tibetan Plateau. *Glob. Chang. Biol.* **2015**, *21*, 3647–3656. [CrossRef]
92. Baniya, B.; Tang, Q.; Huang, Z.; Sun, S.; Techato, K.A. Spatial and temporal variation of NDVI in response to climate change and the implication for carbon dynamics in Nepal. *Forests* **2018**, *9*, 326. [CrossRef]
93. Zhang, Y.; Li, T.; Wang, B. Decadal change of the spring snow depth over the Tibetan Plateau: The associated circulation and influence on the East Asian summer monsoon. *J. Clim.* **2004**, *17*, 2780–2793. [CrossRef]
94. Jin, L.; Ganopolski, A.; Chen, F.; Claussen, M.; Wang, H. Impacts of snow and glaciers over Tibetan Plateau on Holocene climate change: Sensitivity experiments with a coupled model of intermediate complexity. *Geophys. Res. Lett.* **2005**, *32*, L17709. [CrossRef]
95. Yang, K.; Ye, B.; Zhou, D.; Wu, B.; Foken, T.; Qin, J.; Zhou, Z. Response of hydrological cycle to recent climate changes in the Tibetan Plateau. *Clim. Chang.* **2011**, *109*, 517–534. [CrossRef]
96. Peng, J.; Liu, Z.; Liu, Y.; Wu, J.; Han, Y. Trend analysis of vegetation dynamics in Qinghai–Tibet Plateau using Hurst Exponent. *Ecol. Indic.* **2012**, *14*, 28–39. [CrossRef]
97. Zhang, H.; Zhang, Y.L.; Wang, Z.F.; Ding, M.J. Heavy metal enrichment in the soil along the Delhi-Ulan section of the Qinghai-Tibet railway in China. *Environ. Monit. Assess* **2013**, *185*, 5435–5447. [CrossRef]
98. Zhang, L.; Guo, H.; Ji, L.; Lei, L.; Wang, C.; Yan, D.; Li, B.; Li, J. Vegetation greenness trend (2000 to 2009) and the climate controls in the Qinghai-Tibetan Plateau. *J. Appl. Remote Sens.* **2013**, *7*, 073572. [CrossRef]
99. Cong, N.; Shen, M.; Yang, W.; Yang, Z.; Zhang, G.; Piao, S. Varying responses of vegetation activity to climate changes on the Tibetan Plateau grassland. *Int. J. Biometeorol.* **2017**, *61*, 1433–1444. [CrossRef] [PubMed]
100. Granero, M.S.; Segovia, J.T.; Pérez, J.G. Some comments on Hurst exponent and the long memory processes on capital markets. *Phys. Stat. Mech. Appl.* **2008**, *387*, 5543–5551. [CrossRef]
101. Ran, Q.; Hao, Y.; Xia, A.; Liu, W.; Hu, R.; Cui, X.; Xue, K.; Song, X.; Xu, C.; Ding, B.; et al. Quantitative assessment of the impact of physical and anthropogenic factors on vegetation spatial-temporal variation in northern Tibet. *Remote Sens.* **2019**, *11*, 1183. [CrossRef]
102. Li, L.; Zhang, Y.; Wu, J.; Li, S.; Zhang, B.; Zu, J.; Zhang, H.; Ding, M.; Paudel, B. Increasing sensitivity of alpine grasslands to climate variability along an elevational gradient on the Qinghai-Tibet Plateau. *Sci Total Environ.* **2019**, *678*, 21–29. [CrossRef]
103. Mountain Research Initiative EDW Working Group. Elevation-dependent warming in mountain regions of the world. *Nat. Clim Chang.* **2015**, *5*, 424–430. [CrossRef]
104. Nogués-Bravo, D.; Araújo, M.B.; Errea, M.P.; Martínez-Rica, J.P. Exposure of global mountain systems to climate warming during the 21st Century. *Glob. Environ. Chang.* **2007**, *17*, 420–428. [CrossRef]
105. Shen, M.; Piao, S.; Jeong, S.J.; Zhou, L.; Zeng, Z.; Ciais, P.; Chen, D.; Huang, M.; Jin, C.-S.; Li, L.Z.X.; et al. Evaporative cooling over the Tibetan Plateau induced by vegetation growth. *Proc. Natl. Acad. Sci. USA* **2015**, *112*, 9299–9304. [CrossRef]
106. Gao, Y.; Zhou, X.; Wang, Q.; Wang, C.; Zhan, Z.; Chen, L.; Yan, J.; Qu, R. Vegetation net primary productivity and its response to climate change during 2001–2008 in the Tibetan Plateau. *Sci. Total Environ.* **2013**, *444*, 356–362. [CrossRef]
107. Lehnert, L.W.; Wesche, K.; Trachte, K.; Reudenbach, C.; Bendix, J. Climate variability rather than overstocking causes recent large scale cover changes of Tibetan pastures. *Sci. Rep.* **2016**, *6*, 24367. [CrossRef]
108. Shen, M.; Piao, S.; Chen, X.; An, S.; Fu, Y.H.; Wang, S.; Cong, N.; Janssens, I.A. Strong impacts of daily minimum temperature on the green-up date and summer greenness of the Tibetan Plateau. *Glob. Chang. Biol.* **2016**, *22*, 3057–3066. [CrossRef]

109. Zhu, Z.; Piao, S.; Myneni, R.B.; Huang, M.; Zeng, Z.; Canadell, J.G.; Ciais, P.; Sitch, S.; Friedlingstein, P.; Arneth, A.; et al. Greening of the Earth and its drivers. *Nat. Clim. Chang.* **2016**, *6*, 791–795. [CrossRef]
110. Fern´andez-Pascual, E.; Carta, A.; Mondoni, A.; Cavieres, L.A.; Rosbakh, S.; Venn, S.; Satyanti, A.; Guja, L.; Briceño, V.F.; Vandelook, F.; et al. The seed germination spectrum of alpine plants: A global meta-analysis. *New Phytol.* **2021**, *229*, 3573–3586. [CrossRef]
111. Qi, W.; Zhang, Y.; Gao, J.; Yang, X.; Liu, L.; Khanal, N.R. Climate change on the southern slope of Mt. Qomolangma (Everest) Region in Nepal since 1971. *J. Geogr. Sci.* **2013**, *23*, 595–611. [CrossRef]
112. Liang, E.; Dawadi, B.; Pederson, N.; Eckstein, D. Is the growth of birch at the upper timberline in the Himalayas limited by moisture or by temperature? *Ecology* **2014**, *95*, 2453–2465. [CrossRef]
113. Ichiyanagi, K.; Yamanaka, M.D.; Muraji, Y.; Vaidya, B.K. Precipitation in Nepal between 1987 and 1996. *Int. J. Climatol.* **2007**, *27*, 1753–1762. [CrossRef]
114. Putkonen, J.K. Continuous snow and rain data at 500 to 4400 m altitude near Annapurna, Nepal, 1999–2001. *Arct. Antarct. Alp. Res.* **2004**, *36*, 244–248. Available online: http://www.jstor.org/stable/1552167 (accessed on 13 May 2023). [CrossRef]
115. Jeong, S.J.; Ho, C.H.; Gim, H.J.; Brown, M.E. Phenology shifts at start vs. end of growing season in temperate vegetation over the Northern Hemisphere for the period 1982–2008. *Glob. Chang. Biol.* **2011**, *17*, 2385–2399. [CrossRef]
116. Jeong, S.J.; Ho, C.H.; Brown, M.E.; Kug, J.S.; Piao, S. Browning in desert boundaries in Asia in recent decades. *J. Geophys. Res.* **2011**, *116*, D02103. [CrossRef]
117. Liu, L.B.; Zhang, Y.T.; Wu, S.Y.; Li, S.C.; Qin, D.H. Water memory effects and their impacts on global vegetation productivity and resilience. *Sci. Rep.* **2018**, *8*, 2962. [CrossRef]
118. Batllori, E.; Gutiérrez, E. Regional tree line dynamics in response to global change in the Pyrenees. *J. Ecol.* **2008**, *96*, 1275–1288. [CrossRef]
119. Piper, F.I.; Viñegla, B.; Linares, J.C.; Camarero, J.J.; Cavieres, L.A.; Fajardo, A. Mediterranean and temperate treelines are controlled by different environmental drivers. *J. Ecol.* **2016**, *104*, 691–702. [CrossRef]
120. Graham, E.; Mulkey, S.S.; Kitajima, K.; Phillips, N.G.; Wright, S.J. Cloud cover limits net CO2 uptake and growth of a rainforest tree during tropical rainy seasons. *Proc. Natl. Acad. Sci. USA* **2003**, *100*, 572–576. [CrossRef] [PubMed]
121. Carlson, T. An overview of the "Triangle Method" for estimating surface evapotranspiration and soil moisture from satellite imagery. *Sensors* **2007**, *7*, 1612–1629. [CrossRef]
122. Bajracharya, S.R.; Maharjan, S.B.; Shrestha, F.; Guo, W.; Liu, S.; Immerzeel, W.; Shrestha, B. The glaciers of the Hindu Kush Himalayas: Current status and observed changes from the 1980s to 2010. *Int. J. Water Res. Dev.* **2015**, *31*, 161–173. [CrossRef]
123. Li, G.; Lin, H.; Ye, Q. Heterogeneous decadal glacier downwasting at the Mt. Everest (Qomolangma) from 2000 to similar to 2012 based on multi-baseline bistatic SAR interferometry. *Remote Sens. Environ.* **2018**, *206*, 336–349. [CrossRef]
124. Liu, L.L.; Zhang, X.Y.; Donnelly, A.; Liu, X.J. Interannual variations in spring phenology and their response to climate change across the Tibetan Plateau from 1982 to 2013. *Int. J. Biometeorol.* **2016**, *60*, 1563–1575. [CrossRef]
125. Liu, L.B.; Wang, Y.; Wang, Z.; Li, D.L.; Zhang, Y.T.; Qin, D.; Li, S.C. Elevation-Dependent Decline in Vegetation Greening Rate Driven by Increasing Dryness Based on Three Satellite NDVI Datasets on the Tibetan Plateau. *Ecol. Indic.* **2019**, *107*, 105569. [CrossRef]
126. Wessels, K.J.; Prince, S.D.; Malherbe, J.; Small, J.; Frost, P.E.; VanZyl, D. Can human-induced land degradation be distinguished from the effects of rainfall variability? A case study in South Africa. *J. Arid Environ.* **2006**, *68*, 271–297. [CrossRef]
127. Peteet, D. Sensitivity and rapidity of vegetational response to abrupt climate change. *Proc. Natl. Acad. Sci. USA* **2000**, *97*, 1359–1361. [CrossRef]
128. Pearson, R.G.; Phillips, S.J.; Loranty, M.M.; Beck, P.S.A.; Damoulas, T.; Knight, S.J.; Goetz, S.J. Shifts in Arctic vegetation and associated feedbacks under climate change. *Nat. Clim. Chang.* **2013**, *3*, 673–677. [CrossRef]
129. Guo, D.; Zhang, H.Y.; Hou, G.L.; Zhao, J.J.; Liu, D.Y.; Guo, X.Y. Topographic controls on alpine treeline patterns on Changbai Mountain, China. *J. Mt. Sci. Engl.* **2014**, *11*, 429–441. [CrossRef]
130. Körner, C. Alpine Plant Life: Functional Plant Ecology of High Mountain Ecosystems. *Springer Nat.* **2021**, *41*, 53–85. [CrossRef]
131. Sterling, S.M.; Ducharne, A.; Polcher, J. The impact of global land-cover change on the terrestrial water cycle. *Nat. Clim. Chang.* **2013**, *3*, 385–390. [CrossRef]
132. Pan, H.; Li, M.; Cai, X.; Wu, J.; Du, Z.; Liu, X. Responses of growth and ecophsiology of plants to altitude. *Ecol. Environ. Sci.* **2009**, *18*, 722–730.
133. Chen, X.; Ciais, P.; Maignan, F.; Zhang, Y.; Bastos, A.; Liu, L.; Bacour, C.; Fan, L.; Gentine, P.; Goll, D.; et al. Vapor Pressure Deficit and Sunlight Explain Seasonality of Leaf Phenology and Photosynthesis Across Amazonian Evergreen Broadleaved Forest. Global Biogeochem. *Cycles* **2021**, *35*, 6. [CrossRef]
134. Frank, D.; Reichstein, M.; Bahn, M.; Thonicke, K.; Frank, D.; Mahecha, M.D.; Smith, P.; Velde, M.; Vicca, S.; Babst, F.; et al. Effects of climate extremes on the terrestrial carbon cycle: Concepts, processes and potential future impacts. *Glob. Chang. Biol.* **2015**, *21*, 2861–2880. [CrossRef]
135. Yirdaw, E.; Starr, M.; Negash, M.; Yimer, F. Influence of topographic aspect on floristic diversity, structure and treeline of afromontane cloud forests in the Bale Mountains, Ethiopia. *J. For. Res.* **2015**, *26*, 919–931. [CrossRef]
136. Wang, W.; Körner, C.; Zhang, Z.; Wu, R.; Geng, Y.; Shi, W.; Ou, X. No slope exposure effect on alpine treeline position in the Three Parallel Rivers Region, SW China. *Alp. Bot.* **2013**, *123*, 87–95. [CrossRef]

137. Li, X.; Perry, G.L.W.; Brierley, G.J. A spatial simulation model to assess controls upon grassland degradation on the Qinghai-Tibet Plateau, China. *Appl. Geogr.* **2018**, *98*, 166–176. [CrossRef]
138. Yuan, Q.; Yuan, Q.; Ren, P. Coupled effect of climate change and human activities on the restoration/degradation of the Qinghai-Tibet Plateau grassland. *J. Geogr. Sci.* **2021**, *31*, 1299–1327. [CrossRef]
139. Cui, Y.; Li, S.; Yu, C.; Tian, Y.; Zhong, Z.; Wu, J. Effects of the award-allowance payment policy for natural grassland conservation on income of farmer and herdsman families in Tibet. *Acta Pratacult. Sin.* **2017**, *26*, 22–32. [CrossRef]
140. Chen, B.; Zhang, X.; Tao, J.; Wu, J.; Wang, J.; Shi, P.; Zhang, Y.; Yu, C. The impact of climate change and anthropogenic activities on alpine grassland over the Qinghai-Tibet Plateau. *Agric. For. Meteorol.* **2014**, *189*, 11–18. [CrossRef]
141. Cai, H.; Yang, X.; Xu, X. Human-induced grassland degradation/restoration in the central Tibetan Plateau: The effects of ecological protection and restoration projects. *Ecol. Eng.* **2015**, *83*, 112–119. [CrossRef]
142. Xu, H.J.; Wang, X.P.; Zhang, X.X. Alpine grasslands response to climatic factors and anthropogenic activities on the Tibetan Plateau from 2000 to 2012. *Ecol. Eng.* **2016**, *92*, 251–259. [CrossRef]
143. Zhao, H.; Liu, S.; Dong, S.; Su, X.; Wang, X.; Wu, X.; Wu, L.; Zhang, X. Analysis of vegetation change associated with human disturbance using MODIS data on the rangelands of the Qinghai-Tibet Plateau. *Rangel. J.* **2015**, *37*, 77–87. [CrossRef]